NACA TN 1932

9368

TECH LIBRARY KAFB, NM
0065350

NATIONAL ADVISORY COMMITTEE FOR AERONAUTICS

TECHNICAL NOTE 1932

TWO-DIMENSIONAL COMPRESSIBLE FLOW IN CENTRIFUGAL COMPRESSORS WITH STRAIGHT BLADES

By John D. Stanitz and Gaylord O. Ellis

Lewis Flight Propulsion Laboratory
Cleveland, Ohio

Washington
August 1949

AFMDC
TECHNICAL LIBRARY
AFL 2811

319.98/2

TECH LIBRARY KAFB, NM
0065350

NATIONAL ADVISORY COMMITTEE FOR AERONAUTICS

TECHNICAL NOTE 1932

TWO-DIMENSIONAL COMPRESSIBLE FLOW IN CENTRIFUGAL COMPRESSORS WITH STRAIGHT BLADES

By John D. Stanitz and Gaylord O. Ellis

SUMMARY

Six numerical examples are presented for steady, two-dimensional, compressible, nonviscous flow in centrifugal compressors with straight blades, the center lines of which generate a right circular cone when rotated about the axis of the compressor. A seventh example is presented for incompressible flow. The solutions were obtained in a region of the compressors, including the impeller tip, that was considered to be unaffected by diffuser vanes or by the inlet configuration of the impellers. Each solution applies to radial- and conical-flow compressors with various cone angles but with the same included passage angle between blades. (The solutions also apply to radial- and conical-flow turbines with the rotation and flow direction reversed.) The effects of variations in the following parameters were investigated: (1) flow rate, (2) impeller-tip speed, (3) variation of passage height with radius, and (4) number of blades. The numerical results are presented in plots of the streamlines, constant Mach number lines, and constant pressure-ratio lines.

Correlation equations are developed whereby the flow conditions in any impeller with straight blades can be determined (in the region investigated by this analysis) for all operating conditions. As examples of the information provided by the correlation equations, the velocities along the blade surfaces are presented for a wide range of impeller-tip Mach number, flow coefficient, and included passage angle.

INTRODUCTION

At the present time, the design of centrifugal compressors is primarily an art, rather than a science. Little detailed knowledge of flow conditions within the compressor is available upon which to base a rational design. If these flow conditions could be determined, design methods might be developed for centrifugal compressors with higher aerodynamic efficiency and better over-all performance. For

example, the compressor efficiency would be improved if favorable velocity distributions (from the standpoint of boundary-layer growth and separation) could be obtained along the flow surfaces by proper design of the compressor.

For a given set of design and operating parameters, the velocities and pressures within the compressor depend on the three-dimensional flow path and on the fluid properties (compressibility and viscosity). A complete analysis of the flow must include all these factors. If flow conditions are essentially uniform in one direction, however, the flow is adequately represented by a two-dimensional analysis in which the fluid is considered inviscid but compressible. Viscosity of the fluid is unimportant except within the boundary layer along the flow surfaces and this boundary layer is thin provided favorable velocity distributions exist within the compressor. On the other hand, compressibility of the fluid is important in centrifugal compressors because the large pressure ratios per stage result in density changes that affect the fluid velocities, streamlines, and so forth.

In a previous report (reference 1), a general method of analysis was developed for steady, two-dimensional, compressible flow through conical-flow compressors and turbines in which the center line of the passage generates a right circular cone about the axis of rotation. The radial-discharge centrifugal compressor is a special case in which the cone angle is 180°.

In the present report, these analytical methods are applied to investigate the flow conditions within a certain region of radial- or conical-flow compressors and turbines with straight blades. The region investigated includes the impeller tip and is that region which was considered to be unaffected by the inlet configuration of the impeller and by the diffuser vanes; that is, the impeller inlet and the diffuser vanes, if any, must be far enough removed from the region investigated not to affect the flow appreciably in that region. Straight blades were selected because they were considered the most representative blade shape now in use for aircraft centrifugal compressors.

The purpose of this analysis was to determine the effect of operating and design variables (impeller-tip speed, compressor flow rate, variation of passage height with radius, and included passage angle) on flow conditions within the region investigated. From this information, limitations can be placed upon the operating and design variables if certain flow conditions are desired within these regions. For example, if, from boundary-layer considerations,

maximum rates of deceleration of the relative velocity are specified along the flow surfaces, then the results of this analysis can be used to determine limiting values of impeller-tip speed, compressor flow rate, variation of passage height with radius, and included passage angle.

1147

The theoretical investigation presented herein was conducted at the NACA Lewis laboratory.

METHOD OF SOLUTION

Equations

A general analysis was developed in reference 1 for steady, two-dimensional, compressible flow in centrifugal compressors with arbitrary blade shapes and arbitrary variations in the passage height. The analysis is limited to radial- and conical-flow compressors in which the center line of the passage generates a right circular cone when rotated about the axis of the compressor (fig. 1). The two-dimensional flow pattern is considered to lie on the surface of this cone. The final equations, developed in reference 1, are presented in this section together with a brief discussion of the coordinate system and the assumptions and limitations of the analysis.

Coordinate system. - A developed view of the conic surface generated by the passage center line (fig. 1) is shown in figure 2. The dimensionless conic coordinates of a fluid particle on the conic surface are R and θ. (All symbols are defined in appendix A.) The conic-radius ratio R is defined by

$$R = \frac{r}{r_T} \tag{1}$$

where r is the conic radius (distance along conic element from apex of cone) and the subscript T refers to the impeller tip. The coordinate system (R, θ) rotates with the angular velocity ω of the impeller. The passage-height ratio H in the direction normal to the conic surface (fig. 2) is a continuous function of the conic-radius ratio R.

$$H = \frac{h}{h_T} = f(R) \tag{2}$$

where h is the passage height at any conic-radius ratio R.

Assumptions and limitations. - This analysis assumes that flow conditions are uniform across the passage normal to the conic surface; that is, the flow varies only along the conic surface. In order to satisfy this assumption, it is necessary that: (1) the gradient of h with respect to r be small; and (2) the cone angle α be sufficiently large. The allowable variation in α from 180° will depend on the ratio h/r and on the desired accuracy. For the hypothetical limiting case in which h/r approaches zero everywhere along the conic surface, the analysis is accurate for all values of α.

1147

Velocity-ratio components. - The fluid particle on the developed conic surface in figure 2 has a relative tangential velocity ratio U and a radial (along conic element) velocity ratio V. These velocity ratios are defined by

$$U = \frac{u}{c_o} \tag{3a}$$

and

$$V = \frac{v}{c_o} \tag{3b}$$

where

u tangential component of velocity relative to impeller (positive in direction of rotation)

v radial (along conic element) component of velocity

c local speed of sound

Subscript:

o absolute inlet stagnation condition.

Stream function ψ. - A dimensionless stream function ψ satisfies the continuity equation if defined as

$$\frac{\partial\psi}{\partial\theta} = \frac{\rho}{\rho_o} VHR \tag{4a}$$

1147

and

$$\frac{\partial\psi}{\partial R} = \frac{\rho}{\rho_o} UH \tag{4b}$$

where ρ is the weight density.

The stream function ψ is constant along the blade surface. If ψ and θ are assigned values of zero along the driving face of the blade (the blade surface in the direction of rotation), then the value of ψ along the trailing face of the blade (the blade surface opposed to the direction of rotation) is given by

$$\psi_t = \varphi\theta_t \tag{5}$$

where

$$\varphi = \frac{W}{\rho_o a_T c_o} \tag{6}$$

where

$$a_T = B\theta_t r_T h_T \tag{7}$$

where

φ compressor flow coefficient

W compressor flow rate

a flow area (normal to conic surface)

B number of passages (or blades)

Subscript:

t trailing face of blade (blade surface opposed to direction of rotation)

Differential equation. - The differential equation for the stream-function distribution in compressors with straight blades (lying along conic elements) is given by equation (36) of reference 1 in terms of transformed coordinates ξ and η.

1147

$$\frac{2M_T}{\varphi^2}\frac{\rho}{\rho_o}\exp\left[(m+2)\frac{\xi}{\varphi}\right] = \frac{\partial^2\psi}{\partial\xi^2} + \frac{\partial^2\psi}{\partial\eta^2} - \frac{\partial\psi}{\partial\xi}\frac{\partial(\log_e\frac{\rho}{\rho_o})}{\partial\xi} -$$

$$\frac{\partial\psi}{\partial\eta}\frac{\partial(\log_e\frac{\rho}{\rho_o})}{\partial\eta} - \frac{m}{\varphi}\frac{\partial\psi}{\partial\xi} \tag{8}$$

where the impeller-tip Mach number M_T is defined as

$$M_T = \frac{\omega r_T \sin\frac{\alpha}{2}}{c_o} \tag{9}$$

The transformed coordinates ξ and η, which are related to R and θ by

$$\xi = \varphi \log_e R \tag{10a}$$

$$\eta = \varphi\theta \tag{10b}$$

have been introduced because they result in parallel blades in the transformed plane. Such a transformation is desirable because it simplifies the solution of the differential equation by relaxation methods.

In equation (8), the blade-height ratio H is assumed to vary with the conic-radius ratio according to

$$H = R^m \tag{11}$$

where m is an arbitrary exponent. (For $m = 0$ the blade height remains constant and for $m = -1.0$ the flow area remains constant.)

In order to solve equation (8), it is necessary to know the density ratio, which is related to the impeller-tip Mach number and the relative velocity ratio Q by (equation (11), reference 1)

$$\frac{\rho}{\rho_o} = \left\{1 + \frac{\gamma-1}{2}\left[(RM_T)^2 - Q^2\right]\right\}^{\frac{1}{\gamma-1}} \tag{12}$$

where γ is the ratio of specific heats, where

$$Q^2 = U^2 + V^2 \tag{13}$$

and where the absolute whirl of the fluid ahead of the impeller is assumed to be zero. The velocity Q (multiplied by ρ/ρ_o) is in turn given by equations (4), (10), (11), and (13)

$$\frac{\rho}{\rho_o} Q = \frac{\varphi}{\exp\left[(m+1)\frac{\xi}{\Phi}\right]} \left[\left(\frac{\partial\psi}{\partial\xi}\right)^2 + \left(\frac{\partial\psi}{\partial\eta}\right)^2\right]^{1/2} \tag{14}$$

Equations (8), (12), and (14) provide three equations with three unknowns ρ/ρ_o, Q, and ψ.

Numerical procedure

The system of equations (8), (12), and (14) is solved by relaxation methods to obtain the stream-function distribution within the compressor. From this distribution the velocity components and other conditions can be determined using equations (4), and so forth. Detailed outlines for the numerical procedure are given in references 1 and 2. The procedure is sketched briefly herein and an improved technique for satisfying the Kutta condition at the blade tip is discussed in detail.

Outline of procedure. - In order to solve the system of equations by relaxation methods, the following procedure is followed:

(1) Equations (8) and (14) are changed to finite difference form (to be discussed).

(2) Values of ψ are specified on the boundaries of the flow region.

(3) Values of ψ are estimated at equally spaced points of a grid system within the boundaries of the flow region.

(4) The preceding estimated values of ψ are adjusted (relaxed) by the relaxation process until they satisfy equation (8) in finite difference form.

(5) The boundary values of ψ in the vaneless diffuser are adjusted to satisfy the Kutta condition for tangency of flow leaving the tip of the impeller blade.

(6) After the Kutta condition has been satisfied, the grid spacing is reduced near the impeller tip in order to obtain detailed knowledge of the flow characteristics in this region where conditions are rapidly changing.

Finite-difference equations. - Equation (8) is changed to the following finite-difference form (reference 1):

$$\psi_1 + \psi_2 + \psi_3 + \psi_4 - 4\psi - \frac{(\psi_1 - \psi_3)}{4}\left(\log_e \frac{\rho_1}{\rho_o} - \log_e \frac{\rho_3}{\rho_o}\right) -$$

$$\frac{(\psi_4 - \psi_2)}{4}\left(\log_e \frac{\rho_4}{\rho_o} - \log_e \frac{\rho_2}{\rho_o}\right) - \frac{mb}{2\varphi}(\psi_1 - \psi_3) -$$

$$\frac{2M_T}{\varphi^2}\frac{\rho}{\rho_o}\exp\left[(m+2)\frac{\xi}{\varphi}\right]b^2 = \mathscr{R} \tag{15}$$

where

b	grid spacing (fig. 3)
$\mathscr{R}$	residual (error) due to estimated values of ψ used during relaxation solution

Subscripts:

1, 2, 3, and 4	quantities at adjacent grid points as defined in figure 3. (Quantities without numerical subscripts refer to grid point at which $\mathscr{R}$ is being computed.)

From equation (12), the natural logarithm of the density ratio (required for the solution of equation (15)) is plotted as a function of the flow-rate ratio $Q\rho/\rho_o$ in figure 4. The flow-rate ratio is obtained from equation (14), which in finite-difference form becomes

$$\frac{\rho}{\rho_o} Q = \frac{\varphi \left[(\psi_1 - \psi_3)^2 + (\psi_4 - \psi_2)^2\right]^{\frac{1}{2}}}{2b \exp\left[(m+1)\frac{\xi}{\varphi}\right]} \tag{16}$$

Boundary values of ψ. - The stream function ψ is constant along the blade surfaces. If the value of ψ is arbitrarily set equal to zero along the driving face, the value along the trailing face is given by equation (5). Values of ψ along the left bound (fig. 5) are obtained from the simplified analysis of reference 1, which assumes that the flow is parallel to the blade surfaces. Values of ψ along the boundaries of constant η in the vaneless diffuser are estimated by a one-dimensional analysis of the flow (reference 1), which assumes the moment of momentum constant. (Note that these boundary values of ψ in the diffuser are only approximate and must therefore be relaxed along with the values of ψ at interior grid points, as indicated in reference 1.) For all values of ξ in the vaneless diffuser the values of ψ along the boundary $\eta = \eta_t$ are ψ_t greater than the values of ψ along the boundary $\eta = 0$. The values of ψ along the right bound of the diffuser (fig. 5) vary linearly.

Estimated interior values of ψ. - Correlation equations developed in this report (and presented in a later section) provide a first approximation for ψ at grid points within the impeller passage. The error in these estimated values of ψ will, in most cases, be less than ±1 percent of ψ_t.

Relaxation process. - The residuals $\mathscr{R}$ that result from the estimated interior values of ψ are computed at each grid point by equation (15). These residuals are then reduced (relaxed) by suitable changes in the values of ψ. The detailed procedure is given in references 1 and 2.

Kutta condition. - The Kutta condition requires that the streamline leaving the blade surface be tangent to the blade tip. This condition generally is not satisfied by the initial relaxation solution because for this solution the boundary values of ψ along the right bound in the vaneless diffuser (fig. 5) are obtained from the estimated variation in ψ along the boundaries of constant η in the diffuser (discussed in section Boundary values of ψ). In order to satisfy the Kutta condition, the values of ψ along the right bound (ψ_r) must all be changed the same required amount (which amount shall be indicated as $\Delta\psi_r$). This change in ψ_r (that is, $\Delta\psi_r$) results in changes in ψ (that is, $\Delta\psi$) at each of the interior grid points. The manner in which the values of ψ are changed by a change in ψ_r must satisfy the difference equation (15). Therefore,

$$(\psi_1 + \Delta\psi_1) + (\psi_2 + \Delta\psi_2) + (\psi_3 + \Delta\psi_3) + (\psi_4 + \Delta\psi_4) - 4(\psi + \Delta\psi) -$$

$$\frac{(\psi_1 + \Delta\psi_1) - (\psi_3 + \Delta\psi_3)}{4}\left(\log_e \frac{\rho_1}{\rho_o} - \log_e \frac{\rho_3}{\rho_o}\right) -$$

$$\frac{(\psi_4 + \Delta\psi_4) - (\psi_2 + \Delta\psi_2)}{4}\left(\log_e \frac{\rho_4}{\rho_o} - \log_e \frac{\rho_2}{\rho_o}\right) -$$

$$\frac{mb}{2\varphi}\left[(\psi_1 + \Delta\psi_1) - (\psi_3 + \Delta\psi_3)\right] - \frac{2M_T}{\varphi^2}\frac{\rho}{\rho_o}\exp\left[(m + 2)\frac{\xi}{\varphi}\right]b^2 = \mathscr{R} \tag{17}$$

where the change in density ratio resulting from $\Delta\psi$ is considered negligible. Subtracting equation (15) with $\mathscr{R}$ equal to zero (which condition has been satisfied by the initial relaxation) from equation (17) results in

$$\Delta\psi_1 + \Delta\psi_2 + \Delta\psi_3 + \Delta\psi_4 - 4\Delta\psi - \frac{\Delta\psi_1 - \Delta\psi_3}{4}\left(\log_e \frac{\rho_1}{\rho_o} - \log_e \frac{\rho_3}{\rho_o}\right) -$$

$$\frac{\Delta\psi_4 - \Delta\psi_2}{4}\left(\log_e \frac{\rho_4}{\rho_o} - \log_e \frac{\rho_2}{\rho_o}\right) - \frac{mb}{2\varphi}(\Delta\psi_1 - \Delta\psi_3) = \mathscr{R} \tag{17a}$$

Each of the last three terms on the left side of equation (17a) consists of the product of two quantities that approach zero as the grid spacing b approaches zero. For the small grid spacing used in relaxation solutions, these terms are therfore of secondary importance and may be neglected so that

$$\Delta\psi_1 + \Delta\psi_2 + \Delta\psi_3 + \Delta\psi_4 - 4\Delta\psi = \mathscr{R} \tag{17b}$$

The solution of this equation determines $\Delta\psi$ at every grid point for a specified value of $\Delta\psi_r$ (along the right bound of the diffuser). The linearity of equation (17b) permits the solution for any specified $\Delta\psi_r$ to be obtained from the solution for $\Delta\psi_r$ equal to unity by

means of a single multiplying factor, which factor is equal to the specified value of $\Delta\psi_r$. That is, $\Delta\psi$ (at any grid point) resulting from a specified $\Delta\psi_r$ is equal to $\Delta\psi_r$ multiplied by the value of $\Delta\psi$ (at any grid point) resulting from a $\Delta\psi_r$ equal to unity.

The procedure for the solution of equation (17b) is exactly the same as for equation (15). The boundary values of ψ along the blade surfaces and along the left bound (fig. 5) are not changed so that $\Delta\psi$ must equal zero along these boundaries. The value of $\Delta\psi$ along the right bound (fig. 5) is equal to $\Delta\psi_r$, which is set equal to unity.

The magnitude of $\Delta\psi_r$ required to satisfy the Kutta condition can now be determined as follows: If the flow is tangent to the trailing face of the blade at the tip (Kutta condition), then U equals zero at the tip, which, by equations (4b) and (10a), indicates that

$$\left(\frac{\partial\psi}{\partial\xi}\right)_{t,T} = 0$$

Also, by numerical differentiation

$$\left(\frac{\partial\psi}{\partial\xi}\right)_{t,T} = K_t\psi_t + K_a\psi_a + K_b\psi_b + \ldots$$

where K's are constants that can be determined from tables (reference 3, for example), and where the subscripts a, b, . . . indicate successive grid points along the line η_t extending from the blade tip into the diffuser (fig. 5). From the preceding two equations

$$0 = K_t\psi_t + K_a\psi_a^1 + K_b\psi_b^1 + \ldots$$

where ψ^1 signifies the adjusted values of ψ after the Kutta condition is satisfied. But,

$$\psi^1 = \psi + \Delta\psi^1$$

where ψ is the stream function obtained by the initial relaxation and $\Delta\psi^1$ is the change in ψ that results when the Kutta condition is satisfied. But, from above

$$\Delta\psi^{i} = \Delta\psi_r \, \Delta\psi^{ii}$$

where $\Delta\psi^{ii}$ is the change in ψ (at any grid point) resulting from a unit change in ψ_r ($\Delta\psi_r = 1.0$) and $\Delta\psi_r$ is the multiplying factor, which is equal to the change in ψ_r required to satisfy the Kutta condition. Therefore, from the preceding three equations 1147

$$\Delta\psi_r = \frac{-\left(K_t\psi_t + K_a\psi_a + K_b\psi_b + \ldots\right)}{K_a\Delta\psi_a^{ii} + K_b\Delta\psi_b^{ii} + \ldots}$$

This equation determines the change in ψ_r required to satisfy the Kutta condition. The changes in ψ at all other grid points are obtained by multiplying $\Delta\psi_r$ by the values of $\Delta\psi$ (at each grid point) obtained from the solution of equation (17b) for $\Delta\psi_r$ equal to unity. Because the solution for $\Delta\psi$ is approximate, the resulting values of ψ must usually be relaxed to eliminate small residuals computed by equation (15).

The advantage to this method of satisfying the Kutta condition is that, after the solution for $\Delta\psi$ is obtained (this solution applies to all examples with the same value of θ_t), only one complete relaxation solution need be obtained compared with the three required to satisfy the Kutta condition in reference 1.

RESULTS

Seven numerical examples are presented. One of these examples has been selected as the "standard" and in each of the remaining examples one parameter is varied from the standard conditions as shown in the following table:

Example	φ	M_T	m	θ_t (deg)	Type of flow
Standard	0.5	1.5	-1.0	12	Compressible ($\gamma = 1.4$)
1	0.7	1.5	-1.0	12	Compressible ($\gamma = 1.4$)
2	0.9	1.5	-1.0	12	Compressible ($\gamma = 1.4$)
3	0.5	2.0	-1.0	12	Compressible ($\gamma = 1.4$)
4	0.5	1.5	-1.4	12	Compressible ($\gamma = 1.4$)
5	0.5	1.5	-1.0	18	Compressible ($\gamma = 1.4$)
6	0.5	1.5	-1.0	18	Incompressible

Thus, by comparing the solution for the standard example with one of the nonstandard examples, the effect of the change in a single design or operating parameter upon flow conditions in the compressor can be determined.

These examples are for impellers having straight blades (fig. 6). The solutions were obtained in a region of the compressors (including the impeller tip, see fig. 6) that was considered to be unaffected by the inlet configuration of the impeller and by the diffuser vanes; that is, the diffuser vanes, if any, must be far enough removed from the impeller not to affect the flow region being investigated. Each solution applies, within the limitations imposed by the assumption of two-dimensional flow, to radial- and conical-flow compressors (and turbines) with various cone angles α but with the same included passage angle θ_t (reference 1).

The numerical results are presented in plots of the streamlines, constant Mach number lines, and constant pressure-ratio lines.

Streamlines. - The streamline configurations (relative to the impeller) for the seven examples are shown in figure 7. The streamlines are designated in such a manner (ψ/ψ_t) that the value of a streamline indicates the precentage of the total flow (in the passage), which lies between the streamline and the driving face of the blade. For a given density ratio, the streamline spacing is indicative of the velocities relative to the impeller, with close spacing indicating high velocities and wide spacing indicating low velocities.

The streamlines for the standard example are given in figure 7(a). (An extra copy of this figure is enclosed to enable a direct comparison with the streamlines of the nonstandard examples.) For the design and operating conditions of this example, an eddy has begun to form on the driving face of the blade. This eddy results from negative velocities on and near the blade face. The eddy is attached to the blade and rotates with an angular velocity equal and opposite to the rotational velocity of the impeller. (The motion is not a simple rotation but a combination of rotation and deformation required to satisfy boundary conditions.) In actual practice this eddy is probably unstable and it is desirable to eliminate the eddy by proper changes in the design and operating conditions of the compressor. From an inspection of figure 7, it appears that the eddy can be reduced or eliminated by increasing the flow coefficient φ (figs. 7(b) and 7(c)), decreasing the impeller-tip Mach number M_T (fig. 7(d)), decreasing the included passage angle θ_t (fig. 7(f)) and using incompressible fluids

1147

(fig. 7(g)). The eddy in figure 7(d) (impeller-tip Mach number of 2.0) is especially interesting because it occupies more than half of the available flow area at a radius ratio of 0.90.

The exponent m determines the change in flow area through the impeller and the diffuser. For m equal to -1.4 (example 4), the flow-area ratio (flow area divided by flow area at impeller tip) at a radius ratio of 0.5 is 1.32 compared to a ratio of 1.0 for the standard example (in which m equals -1 0). The effect of m upon the streamline configuration in the flow region investigated is not appreciable (compare figs. 7(a) and 7(e)). The reason for this small effect is that the flow areas at the impeller tip are the same (because φ is the same) and for reasonable values of m are not much different anywhere in the flow region investigated (which is in the vicinity of the tip, fig. 6). If the area ratio 1.32 had been obtained by maintaining equal flow areas for both impellers at the radius ratio 0.5 within the impellers and decreasing the area at the impeller tip in one case, then the streamline configuration would be greatly affected. But this effect would not be the result of the change in m but rather the change in φ (which results from the change in a_T).

The large effect of compressibility upon the streamline configuration (an therefore upon the other flow conditions) is shown by a comparison of figures 7(f) and 7(g). The large eddy that exists for compressible flow completely disappears for incompressible flow. It is apparent that incompressible-flow solutions give a poor qualitative (or quantitative) picture of the flow under these design and operating conditions.

Mach number lines. - Lines of constant Mach number relative to the impeller are shown for the seven examples in figure 8. It should be noted that the Mach number in the incompressible solution (fig. 8(g)) is a fictitious quantity that is equal to the fluid velocity q divided by a constant that is equal to the inlet stagnation speed of sound c_o of whatever compressible solution with which the incompressible solution is being compared. This inlet stagnation speed of sound is also contained in the definitions of ψ and M_T, so that for the incompressible solution q/c_o, φ, and M_T vary inversely with the assigned value of c_o, but ratios of these parameters are unaffected. The standard example is given in figure 8(a). (An extra copy of this figure is enclosed to enable a direct comparison with the nonstandard examples.) The general characteristics of these plots are similar. The velocities (as indicated by the Mach number lines) along the

driving face of the blade are low; the velocities along the trailing face are high; and the velocities become equal on both the driving and trailing faces at the blade tip (as required by the Kutta condition). The maximum Mach number occurs on the trailing face of the blade at a radius ratio well within the impeller and the flow decelerates along the face of the blade from this point to the blade tip. This deceleration, which, for impellers with straight blades and with the usual type of area variation with radius ratio, becomes rapid near the blade tip, is conducive to boundary-layer separation, which lowers the compressor efficiency.

If boundary-layer effects are neglected, the velocities at the impeller tip are reasonably uniform and any nonuniformity becomes negligible at a radius ratio of approximately 1.10 for θ_t equal to 12° (figs. 8(a) to 8(e)) and a radius ratio of approximately 1.15 for θ_t equal to 18° (figs. 8(f) and 8(g)). These radius ratios and their corresponding angles are equivalent to a ratio of ξ/η_t approximately equal to 0.45. Flow conditions in the vaneless portion of the diffuser immediately following the impeller, therefore, become essentially uniform at a ratio of ξ/η_t approximately equal to 0.45. The average relative Mach number at the impeller tip is low (even for large values of φ) because of the high impeller-tip Mach numbers, which result in high fluid densities and therefore low velocities.

From an inspection of figures 8(a) to 8(g), it appears that the maximum Mach number (on the trailing face of the blade) is increased by increasing the flow coefficient φ (figs. 8(b) and 8(c)), is apparently not much affected by increasing the impeller-tip Mach number M_T (fig. 8(d)) or by changing the exponent m (fig. 8(e)), and is increased by increasing the included passage angle θ_t (fig. 8(f)) or by changing to an incompressible fluid (fig. 8(g)), (in which the Mach number is a fictitious quantity as previously indicated).

Lines of constant velocity ratio are shown in figure 9 for example 5. The velocity ratio is the local velocity divided by the speed of sound at absolute inlet stagnation conditions (a constant), which is in contrast to the relative Mach number (fig. 8), which is the local velocity divided by the local speed of sound (a function of R and θ). Figure 9 has been added to show that the plots of Mach number and velocity ratio have the same general characteristics (compare figs. 8(f) and 9) so that valid conclusions regarding the qualitative behavior of the velocities can be drawn from plots of the Mach number.

Pressure-ratio lines. - Lines of constant static-pressure ratio (local pressure divided by absolute inlet stagnation pressure) are shown for the seven examples in figure 10. The standard example is given in figure 10(a). (An extra copy of this figure is enclosed to enable a direct comparison with the nonstandard examples.) The general characteristics of these plots are the same. At a given radius ratio, the pressure ratio is higher on the driving face of the blade than on the trailing face except at the blade tip where the pressure ratios are equal. This difference in pressure ratio accounts for the impeller torque.

Slip factor. - The impeller slip factor is defined as the ratio of the average absolute tangential velocity of the fluid leaving the impeller tip to the tip speed of the impeller. The slip factor has been computed for each of the seven examples by methods given in reference 1. The resulting slip factors are given in the following table:

Example	Nonstandard parameter	Slip factor
Standard	----------	0.934
1	$\varphi = 0.7$	.937
2	$\varphi = 0.9$	.938
3	$M_T = 2.0$	.935
4	$m = -1.4$	.934
5	$\theta_t = 18^\circ$	.899
6	$\rho/\rho_o = 1.0$[a]	.892

[a]$\theta_t = 18^\circ$ also.

It appears that the only variable investigated that affects the computed slip factor is the included passage angle θ_t. In particular, it will be noted that the slip factor is approximately the same for compressible and incompressible flow (compare examples 5 and 6) although the streamline configurations for the two examples are very different (compare figs. 7(f) and 7(g)).

The following comments can be made concerning the dependence of the slip factor on θ_t only: The mean absolute tangential velocity of the fluid leaving the impeller tip (which determines the slip factor) is made up of two parts - that induced by the vortex representing the motion of the impeller, and that induced by the vortex distribution along the blades necessary to satisfy the Kutta condition. It is this second part that causes the slip factor to deviate

from unity. But this second part is associated with the adjustment in ψ_r (that is, $\Delta\psi_r$) required to satisfy the Kutta condition and this adjustment has been found to be independent of φ, M_T, and compressibility and dependent on θ_t only. (See section on Kutta condition.) Hence, it is not surprising that the slip factor is dependent on θ_t only.

CORRELATION OF RESULTS

Correlation equations are presented whereby the flow conditions (U, V, ψ/ψ_t, and so forth) within any impeller with straight blades can be determined (for the flow region investigated herein, see fig. 6) from the flow conditions for the standard solution of this report. These correlation equations are developed in appendix B and the flow conditions for the standard solution are given in tables I, II, and III.

The correlation equations are developed in terms of transformed coordinate ratios (ξ/η_t and η/η_t). The dimensionless conical coordinates R and θ are related to these transformed coordinate ratios by

$$R = \exp\left(\theta_t \frac{\xi}{\eta_t}\right) \tag{B3}$$

and

$$\theta = \theta_t \frac{\eta}{\eta_t} \tag{B4}$$

Stream-function ratio, ψ/ψ_t. - The stream-function ratio ψ/ψ_t varies across the impeller passage from 0 along the driving face of one blade to 1.0 along the trailing face of the next blade. At any given point (ξ/η_t and η/η_t) within the impeller, the value of the stream-function ratio for any impeller (with straight blades) and for any operating condition can be estimated by the following correlation equation (appendix B):

$$\frac{\psi'}{\psi_t} = \frac{\eta}{\eta_t} + \frac{A}{V_m}\left(\left[V_m\left(\frac{\psi}{\psi_t} - \frac{\eta}{\eta_t}\right)\right]_s + \frac{\eta}{\eta_t}\left(\frac{\eta}{\eta_t} - 1\right)\left\{\frac{U_s}{2}\left[\theta_t - (\theta_t)_s\right] + (R-R_s)(M_T\theta_t)_s\right\}\right) \tag{B16}$$

where the prime indicates estimated value of flow condition (stream-function ratio in this case) at a given point $(\xi/\eta_t,\ \eta/\eta_t)$ and the subscript s indicates standard value of flow condition at the same point. Also,

$$A = \frac{M_T\theta_t}{(M_T\theta_t)_s} \tag{B2}$$

$$V_m = \frac{\varphi}{\frac{\rho_m}{\rho_o} RH} \tag{B9}$$

and, if the absolute whirl ahead of the impeller is zero,

$$\frac{\rho_m}{\rho_o} = \left\{1 + \frac{\gamma-1}{2}\left[(RM_T)^2 - \left(\frac{\varphi}{\frac{\rho_m}{\rho_o} RH}\right)^2\right]\right\}^{\frac{1}{\gamma-1}} \tag{B10}$$

where the subscript m indicates the mean value at a given radius ratio R (that is, at a given value of ξ/η_t).

The estimated values of the stream-function ratio ψ'/ψ_t obtained from the correlation equation (B16) are compared in figure 11 with the relaxation values of ψ/ψ_t obtained for the numerical examples of this report. Values are plotted for every other grid point across the passage at values of ξ/η_t indicated by the symbols. Perfect correlation corresponds to the 45° line on this plot. The error is, with very few exceptions, less than 0.01, where the error is defined as

$$\text{Error} = \left(\frac{\psi'}{\psi_t} - \frac{\psi}{\psi_t}\right) \tag{18}$$

The negative values of ψ/ψ_t shown on the correlation plot correspond to eddies, which were shown in the previous section to form on the driving face of the blade at low flow rates and at high tip speeds. The stream-function ratio is always zero at the driving face of the blade and always 1.0 at the trailing face.

1147

Radial-velocity ratio V. - The radial-velocity ratio can be estimated by the following correlation equation (appendix B):

$$V' = V_m + A(V-V_m)_s + A\left[2\left(\frac{\eta}{\eta_t}\right) - 1\right]\left\{\frac{U_s}{2}\left[\theta_t - \left(\theta_t\right)_s\right] + (R-R_s)(M_T\theta_t)_s\right\} \tag{B13}$$

The estimated values of the radial-velocity ratio V' obtained from equation (B13) are compared in figure 12 with the values of V obtained from the relaxation solutions of this report. Values are plotted for every other grid point across the passage at the values of ξ/η_t indicated by the symbols. Perfect correlation corresponds to the 45° line on this plot. The error is less than 0.01 where the error is defined as

$$\text{Error} = (V' - V) \tag{19}$$

The negative values of V shown in the correlation plot correspond to the eddies that form on the driving face of the blade at low flow rates and at high tip speeds.

Tangential-velocity ratio U. - The relative tangential-velocity ratio can be estimated by the following correlation equation (appendix B):

$$U' = AU_s \tag{B1}$$

The estimated values of the relative tangential-velocity ratio U' obtained from equation (B1) are compared in figure 13 with the values of U obtained from the relaxation solutions of this report. Values are plotted for every grid point across the first half of the passage for the values of ξ/η_t indicated by the symbols. Perfect correlation corresponds to the 45° line on this plot. Except for the incompressible solution (example 6), the error is less than 0.01 where the error is defined as

$$\text{Error} = (U' - U) \tag{20}$$

The relative tangential-velocity ratio is always zero along the blade surfaces.

1147

Other flow conditions. - Other flow conditions within the impeller can be determined from the values of U and V obtained by the correlation equations (B1) and (B13). The relative velocity ratio Q is given by

$$Q^2 = U^2 + V^2 \tag{13}$$

From the steady-flow energy equation the temperature ratio is given by (reference 1)

$$\frac{T}{T_o} = 1 + \frac{\gamma-1}{2}\left[(RM_T)^2 - Q^2\right] \tag{21}$$

where T is the absolute static temperature of the gas and where the absolute whirl ahead of the impeller is assumed zero.

The density ratio and the pressure ratio are obtained from the temperature ratio by

$$\frac{\rho}{\rho_o} = \left(\frac{T}{T_o}\right)^{\frac{1}{\gamma-1}} = \left\{1 + \frac{\gamma-1}{2}\left[(RM_T)^2 - Q^2\right]\right\}^{\frac{1}{\gamma-1}} \tag{12}$$

and

$$\frac{p}{p_o} = \left(\frac{T}{T_o}\right)^{\frac{\gamma}{\gamma-1}} = \left\{1 + \frac{\gamma-1}{2}\left[(RM_T)^2 - Q^2\right]\right\}^{\frac{\gamma}{\gamma-1}} \tag{22}$$

The local relative Mach number is related to Q and the temperature ratio by

$$M = \frac{Q}{\sqrt{\frac{T}{T_o}}} \tag{23}$$

Correlation of velocities along blade surfaces. - Of special interest, because of boundary-layer considerations, are the velocity distributions along the trailing and driving faces of the impeller blades, Q_t and Q_d. Estimated values of Q_t obtained from the correlation equations are given by the curves in figure 14 for each of the numerical examples in this report. The values of Q_t obtained by the relaxation solution are shown by the plotted points. The agreement is seen to be excellent in all cases.

Estimated values of Q_d obtained from the correlation equations are given by the curves in figure 15 for each of the numerical examples in this report. The values of Q_d obtained by the relaxation solution are shown by the plotted points. Again the agreement is excellent.

1147

Slip factor. - The impeller slip factor μ is defined as the ratio of the absolute tangential velocity of the fluid leaving the impeller tip to the tip speed of the impeller. The following correlation equation is developed in appendix C for the slip factor of impellers with straight blades:

$$\mu' = 1 - (1 - \mu_s) \frac{\theta_t}{(\theta_t)_s} \tag{C2}$$

For the standard solution, θ_t is 0.2095 radians and μ_s is 0.934 so that the slip factor equation becomes

$$\mu' = 1 - 0.315\ \theta_t \tag{24}$$

This equation is plotted in figure 16 together with Stodola's equation, which for straight blades is given by

$$\mu = 1 - 0.500\ \theta_t \tag{25}$$

The slip factors obtained for the numerical examples of this report are plotted as points in figure 16. These points indicate that the slip factor is independent of flow rate φ, impeller-tip speed M_T, and variation of flow area with radius m and depends only on the included passage angle θ_t. This conclusion is in agreement with Stodola's equation although the magnitude of the slip factor given by Stodola is lower.

APPLICATION OF CORRELATION EQUATIONS

The correlation equations presented in the previous section are important because they provide rapid solutions (in the regions investigated herein, fig. 6) to the differential equation, which determines the flow conditions (U, V, p/p_o, and so forth) in any impeller (with straight blades) for all operating conditions. An important application of the correlation equations is the determination of velocities along the flow surfaces because these

1147

velocities are significant in the study of the boundary layer. As examples of the information provided by the correlation equations for such a study, the velocities along the blade surfaces have been computed over a wide range of impeller-tip Mach number M_T, flow coefficient φ, and included passage angle θ_t. These computations are presented in figures 17 to 19.

Impeller-tip Mach number M_T. - The effect of M_T upon the velocities along the driving and trailing faces of a blade is shown in figure 17. In this figure all design and operating conditions (other than M_T) were maintained constant at the standard values.

For M_T equal to zero the velocities are equal on both faces of the blade. For all other values of M_T the relative velocities are higher on the trailing face than on the driving face and as the impeller-tip speed increases the difference in velocities along the two faces increases. Except near the tip, this increase in velocity difference results primarily from a decrease in velocity along the driving face, and for high values of M_T this velocity becomes negative, which indicates the presence of an eddy. The small effect of M_T upon Q_t results from a combination of effects. At higher values of M_T, the difference between Q_t and the mean radial-velocity ratio V_m increases but V_m itself decreases because of the increased density and the net result is only a small change in Q_t with changes in M_T. At the blade tip the velocity becomes equal on both surfaces, and this velocity decreases with increasing M_T because of the higher gas density.

Flow coefficient φ. - The effect of flow coefficient φ upon the velocities along the driving and trailing faces of a blade is shown in figure 18. In this figure, all design and operating conditions (other than the flow coefficient) were maintained constant at the standard values.

At each radius ratio the difference between Q_t and Q_d is independent of φ (that is, remains constant). The mean radial-velocity ratio V_m, however, decreases with decreasing flow coefficient, and for low flow coefficients Q_d becomes negative, which indicates the presence of an eddy. At the blade tip, the velocity becomes equal on both surfaces and this velocity increases with increasing flow coefficient because of the increased mean radial velocity V_m.

For φ equal to zero the velocities are equal on both surfaces of the blade (but opposite in sign). As a result the pressures on both blade surfaces are equal and no work is done by the impeller. The entire flow within the passage is an eddy.

Passage angle θ_t. - The effect of included passage angle upon the velocities along the driving and trailing faces of a blade is shown in figure 19. In this figure all design and operating conditions (other than the passage angle) were maintained constant at the standard values. Increased values of θ_t indicate fewer blades.

The correlation equation (B13) used to obtain the curves plotted in figure 19 is developed in terms of a dimensionless transformed coordinate ξ/η_t, which is related to the radius ratio R by an expression (equation (B3)) that includes the passage angle θ_t. The minimum value of ξ/η_t for which standard values of U, V, and so forth are given in tables I, II, and III is -1.7030, which for values of θ_t less than standard ($\theta_t = 12^\circ$) corresponds to values of R greater than 0.7, as indicated by equation (B3) and shown in figure 19. However, for values of R less than those resulting from ξ/η_t equal to -1.7030 the simplified analysis presented in reference 1 for impellers with straight blades may be used to extrapolate the curves to all lesser values of R. In terms of the mean velocity ratio V_m (equation (B9)), the simplified equation for the velocity ratio becomes (Note that the simplified analysis of reference 1 assumes U = 0.)

$$Q = V = V_m + RM_T\theta_t\left[2\left(\frac{\theta}{\theta_t}\right) - 1\right] \tag{26}$$

Equation (26) has been used to extrapolate the curves for θ_t less than 12° in figure 19 (dashed lines). For values of ξ/η_t less than -1.7030, the simplified analysis given in reference 1 can be used to determine the flow conditions (V, p/p_o, and so forth) within the impeller passage for any design and operating condition. For values of ξ/η_t greater than -1.7030, the methods of this report must be used to determine V, p/p_o, and so forth.

For θ_t equal to zero the velocities are the same on both surfaces of the blade and are equal to the mean velocity V_m (dashed line). This mean velocity is the same for all values of θ_t, but the difference between V_m and Q_d increases with increasing values of θ_t so that, for large values of θ_t, Q_d becomes negative which indicates the presence of an eddy.

SUMMARY OF RESULTS AND CONCLUSIONS

Six numerical examples are presented for steady, two-dimensional, compressible, nonviscous flow in centrifugal compressors with straight blades, the center lines of which generate a right circular cone when rotated about the axis of the compressor. A seventh example is presented for incompressible flow. The solutions were obtained in a region of the compressors (including the impeller tip) that was considered to be unaffected by the inlet configuration of the impeller and by the diffuser vanes. (That is, the impeller inlet and the diffuser vanes, if any, must be far enough removed from the region investigated not to affect the flow appreciably in that region.) The effects of variations in the following parameters were investigated: (1) flow coefficient (flow rate), (2) impeller-tip Mach number, (3) exponent for the variation of passage height ratio with radius ratio, and (4) the included passage angle. Each solution applies to radial- and conical-flow compressors (and turbines with the rotation and flow direction reversed) with various cone angles but with the same included passage angle. The numerical results are presented in plots of the streamlines, constant Mach number lines, and constant pressure-ratio lines.

Correlation equations are developed whereby the flow conditions (streamlines, velocities, pressures, impeller slip factor, and so forth) within any impeller with straight blades can be determined (for the flow region investigated) from the flow conditions of the standard solution presented. As examples of the information provided by the correlation equations, the velocities along the blade surfaces have been computed (and plotted) over a wide range of impeller-tip Mach number, flow coefficient, and included passage angle.

The principle conclusions resulting from the work presented herein are:

1. The exponent m, which was used in this analysis to specify the variation in flow area with radius ratio, has only a small effect (for practical values of m) upon the area variation in the flow region investigated and therefore has only a small effect upon the flow in this region.

2. An eddy forms on the driving face of the blade at high impeller-tip Mach numbers, low flow coefficients, and large included passage angles. For an impeller-tip Mach number of 2.0 (and the standard values of flow coefficient and included passage angle), the eddy occupies more than 50 percent of the flow area at a radius ratio of 0.90.

3. Compressibility has a great effect upon the streamline configuration within the compressor (and therefore upon the other flow conditions). For example, the large eddy that exists in the compressible-flow example (with the same parameters as the incompressible example) completely disappears in the incompressible example.

4. The maximum relative Mach number occurs on the trailing face of the blade at a radius ratio well within the impeller and the flow decelerates along the face of the blade from this point to the blade tip. This deceleration, which, for impellers with straight blades and with the usual type of area variation with radius ratio, becomes rapid near the blade tip, is conducive to boundary-layer separation.

5. If boundary-layer effects are neglected, the flow conditions in the vaneless diffuser following the impeller become essentially uniform at a coordinate ratio of ξ/η_t approximately equal to 0.45.

6. For the high impeller-tip Mach numbers investigated (and if boundary-layer effects are neglected), the velocities at the impeller tip are low, because the high impeller-tip Mach numbers result in high fluid densities.

7. The maximum relative Mach number (on the trailing face of the blade) is increased by increasing the flow coefficient or the included passage angle (number of blades) but is affected little by the impeller-tip Mach number.

8. The impeller slip factor is independent of the impeller-tip Mach number, compressor flow coefficient, variation in flow area with radius ratio, and compressibility of the fluid. The slip factor is a function of the included passage angle only.

9. The difference between velocities on the trailing and driving faces of the blades increases with increasing tip Mach number and included passage angle but is independent of the flow coefficient.

Lewis Flight Propulsion Laboratory,
National Advisory Committee for Aeronautics,
Cleveland, Ohio, June 21, 1949.

APPENDIX A

The following symbols are used in this report:

A ratio, $\frac{M_T\theta_t}{(M_T\theta_t)_s}$

a flow area, normal to conic surface

B number of passages (or blades)

b grid spacing (fig. 3)

c local speed of sound

exp exponential, $\left[\exp(x) = e^x\right]$

H passage-height ratio, h/h_T

h passage height, normal to conic surface

M local Mach number

M_T impeller-tip Mach number, $\frac{\omega r_T \sin\frac{\alpha}{2}}{c_o}$

m passage-height exponent

p absolute static pressure

Q relative velocity ratio, $\sqrt{U^2 + V^2}$

q relative velocity

R conic-radius ratio, r/r_T

$\mathscr{R}$ residual

r conic radius (distance along conic element from apex of cone)

T absolute static temperature

U relative tangential-velocity ratio, u/c_o

u relative tangential velocity

V radial-velocity ratio, v/c_o

v radial velocity, along conic element

1147

W total compressor flow rate

α cone angle (fig. 1)

γ ratio of specific heats

Δ small change

η transformed coordinate, $\varphi\theta$

θ angle, radians unless otherwise specified

μ impeller slip factor

ξ transformed coordinate, $\varphi \log_e R$

ρ weight density of fluid

φ compressor flow coefficient, $\frac{W}{\rho_o a_T o_o}$

ψ compressible stream function

ω impeller angular velocity

Subscripts:

d driving face of blade (blade surface in direction of rotation)

m mean value at given radius ratio

o absolute inlet stagnation condition

r right bound (fig. 5)

s standard solution

T impeller tip

t trailing face of blade (blade surface opposed to direction of rotation)

1, 2, 3, and 4 grid points adjacent to point being considered (fig. 3)

1147

Superscripts:

$'$ estimated value

ψ^{i} adjusted value of ψ after Kutta condition is satisfied

$\Delta\psi^{i}$ change in ψ resulting from $\Delta\psi_r$ required to satisfy Kutta condition

$\Delta\psi^{ii}$ change in ψ resulting from $\Delta\psi_r$ equal to unity

1147

APPENDIX B

CORRELATION EQUATIONS

Correlation equations are developed whereby the flow conditions (U, V, and ψ/ψ_t) within any impeller with straight blades can be determined from the flow conditions for the standard solution of this report.

Tangential-Velocity Ratio U

A plot of U against η/η_t (equal to θ/θ_t, see equation (10b)) at ξ/η_t equal to 0 for various design and operating conditions (used in the relaxation solutions of this report) is shown in figure 20. These curves are representative examples of the variation in U for all values of ξ/η_t at which U is significant. For a given value of ξ/η_t and η/η_t, the tangential velocity ratio U is seen to be a function of the impeller-tip Mach number M_T and the included passage angle θ_t only. The tangential-velocity ratio is independent of the compressor flow rate (flow coefficient, φ) and the variation of flow area with R (passage-height exponent, m). This dependence of U upon M_T and θ_t only (for a given value of ξ/η_t and η/η_t) was found to exist at all radius ratios at which U is significant and was found to be a direct relation such that

$$U = KM_T\theta_t$$

where K is a function (of ξ/η_t and η/η_t) which is constant for all design and operating conditions. Therefore, in terms of the standard solution

$$U' = AU_s \tag{B1}$$

where

$$A = \frac{M_T\theta_t}{(M_T\theta_t)_s} \tag{B2}$$

and where the subscript s refers to values from the standard example and the prime indicates the estimated value for the nonstandard example. Equation (B1) is the correlation equation for the relative tangential-velocity ratio.

1147

The correlation equation (B1) and the other correlation equations to be developed in this appendix refer to the same transformed coordinate ratios ξ/η_t and η/η_t for both the standard and nonstandard quantities in the equations. From equations (10a) and (10b), these transformed coordinate ratios are related to the coordinate ratios in the physical (R, θ) plane by

$$R = \exp\left(\theta_t \frac{\xi}{\eta_t}\right) \tag{B3}$$

and

$$\theta = \theta_t \frac{\eta}{\eta_t} \tag{B4}$$

Radial-Velocity Ratio V

The correlation equation for the radial-velocity ratio is obtained from the equation for irrotational absolute motion of a fluid particle. From reference 1,

$$-2\omega r_T \sin\frac{\alpha}{2} = \frac{u}{R} + \frac{\partial u}{\partial R} - \frac{1}{R}\frac{\partial v}{\partial \theta}$$

which, after dividing by c_o and multiplying by θ_t, becomes

$$-2M_T\theta_t = \left(\frac{U}{R} + \frac{\partial U}{\partial R}\right)\theta_t - \frac{1}{R}\frac{\partial V}{\partial\left(\frac{\eta}{\eta_t}\right)} \tag{B5}$$

Plots of V against η/η_t for various design and operating conditions and for ratios of ξ/η_t equal to 0 and -1.0 are shown in figure 21. These plots are representative of the variation in V at all values of ξ/η_t within the impeller. The slopes of the velocity profiles $\frac{\partial V}{\partial(\eta/\eta_t)}$ are seen to be nearly constant (except in the immediate vicinity of the blade tip) so that from equation (B5)

$$\left(\frac{U}{R} + \frac{\partial U}{\partial R}\right) = f\left(\frac{\xi}{\eta_t}\text{ only}\right) \tag{B6}$$

and equation (B5) can be integrated to give

$$V = V_d + 2RM_T\theta_t \left(\frac{\eta}{\eta_t}\right) + R\theta_t \left(\frac{U}{R} + \frac{\partial U}{\partial R}\right)\left(\frac{\eta}{\eta_t}\right) \tag{B7}$$

where V equals V_d and η/η_t equals zero along the driving face of the blade.

The velocity ratio V_d can be evaluated from the condition

$$\left.\begin{aligned} V &= V_m \\ \text{when} \qquad \frac{\eta}{\eta_t} &= 0.5 \end{aligned}\right\} \tag{B8}$$

where V_m is the mean radial-velocity ratio, which is obtained from continuity considerations as follows:

$$W = \rho_m v_m rhB\theta_t$$

or

$$\frac{W}{\rho_o a_T c_o} = \varphi = \frac{\rho_m}{\rho_o} V_m RH$$

so that

$$V_m = \frac{\varphi}{\frac{\rho_m}{\rho_o} RH} \tag{B9}$$

The mean density ratio ρ_m/ρ_o in equation (B9) is obtained from equation (12) by assuming that for straight blades the relative tangential velocity is zero and the radial-velocity ratio is equal to the mean radial-velocity ratio V_m

$$Q^2 \approx V_m^2 = \left(\frac{\varphi}{\frac{\rho_m}{\rho_o} RH}\right)^2$$

Equation (12) becomes

$$\frac{\rho_m}{\rho_o} = \left\{1 + \frac{\gamma-1}{2}\left[(RM_T)^2 - \left(\frac{\varphi}{\frac{\rho_m}{\rho_o} RH}\right)^2\right]\right\}^{\frac{1}{\gamma-1}} \tag{B10}$$

Equation (B10) gives an average value of the density ratio, which is assumed to be a function of ξ/η_t (that is, R) and independent of η/η_t (that is, θ/θ_t).

From equation (B7) and the condition given by equations (B8), the velocity ratio V_d becomes

$$V_d = V_m - RM_T\theta_t - \frac{R\theta_t}{2}\left(\frac{U}{R} + \frac{\partial U}{\partial R}\right)$$

and equation (B6) becomes

$$V = V_m + RM_T\theta_t\left[2\left(\frac{\eta}{\eta_t}\right) - 1\right] + \frac{R\theta_t}{2}\left(\frac{U}{R} + \frac{\partial U}{\partial R}\right)\left[2\left(\frac{\eta}{\eta_t}\right) - 1\right] \tag{B11}$$

From equation (B3),

$$\frac{\partial U}{\partial R} = \frac{\partial U}{\partial(\xi/\eta_t)}\frac{d(\xi/\eta_t)}{dR} = \frac{1}{R\theta_t}\frac{\partial U}{\partial(\xi/\eta_t)}$$

and from equation (B1),

$$\left(\frac{U}{R} + \frac{\partial U}{\partial R}\right) = \frac{A}{R\theta_t}\left(\theta_t U_s + \frac{\partial U_s}{\partial(\xi/\eta_t)}\right) \tag{B12}$$

so that equation (B11) becomes

$$V = V_m + RM_T\theta_t\left[2\left(\frac{\eta}{\eta_t}\right) - 1\right] + \frac{A}{2}\left(\theta_t U_s + \frac{\partial U_s}{\partial(\xi/\eta_t)}\right)\left[2\left(\frac{\eta}{\eta_t}\right) - 1\right]$$

which is solved for $\partial U_s/\partial(\xi/\eta_t)$

$$\frac{\partial U_s}{\partial\left(\frac{\xi}{\eta_t}\right)} = \frac{V - V_m}{\frac{A}{2}\left[2\left(\frac{\eta}{\eta_t}\right) - 1\right]} - \frac{2RM_T\theta_t}{A} - \theta_t U_s$$

The term $\partial U_s/\partial(\xi/\eta_t)$ can be eliminated by equating it for the standard and nonstandard cases. Therefore,

$$V' = V_m + A(V-V_m)_s + A\left[2\left(\frac{\eta}{\eta_t}\right) - 1\right]\left\{\frac{U_s}{2}\left[\theta_t - (\theta_t)_s\right] + (R-R_s)(M_T\theta_t)_s\right\} \tag{B13}$$

Equation (B13) is the correlation equation for the radial-velocity ratio.

Stream-Function Ratio ψ/ψ_t

The stream-function ratio is obtained from the definition of the stream function and from the correlation equation for the radial-velocity ratio V. The definition of the stream function is given by equation (4a).

$$\frac{\partial\psi}{\partial\theta} \equiv \frac{\rho}{\rho_o} VHR \tag{4a}$$

which, after being multiplied by θ_t and combined with equation (B11), becomes

$$\frac{\partial\psi}{\partial\left(\frac{\eta}{\eta_t}\right)} = \frac{\rho}{\rho_o} RH\theta_t\left\{V_m + RM_T\theta_t\left[2\left(\frac{\eta}{\eta_t}\right) - 1\right] + \frac{R\theta_t}{2}\left(\frac{U}{R} + \frac{\partial U}{\partial R}\right)\left[2\left(\frac{\eta}{\eta_t}\right) - 1\right]\right\} \tag{B14}$$

From the condition given by equation (B6) and if the density ratio is replaced by its mean value for ξ/η_t, equation (B14) can be integrated to give

$$\frac{\psi}{\psi_t} = \frac{1}{V_m}\left\{V_m + RM_T\theta_t\left[\left(\frac{\eta}{\eta_t}\right) - 1\right] + \frac{R\theta_t}{2}\left(\frac{U}{R} + \frac{\partial U}{\partial R}\right)\left[\left(\frac{\eta}{\eta_t}\right) - 1\right]\right\}\left(\frac{\eta}{\eta_t}\right) \tag{B15}$$

where ψ_t is given by equation (5) and ψ/ψ_t is equal to zero when η/η_t is equal to zero. Introducing equation (B12) and solving for $\partial U_s/\partial(\xi/\eta_t)$ give

$$\frac{\partial U_s}{\partial(\xi/\eta_t)} = \frac{V_m\left(\frac{\psi}{\psi_t} - \frac{\eta}{\eta_t}\right) - RM_T\theta_t\left(\frac{\eta}{\eta_t} - 1\right)\frac{\eta}{\eta_t}}{\frac{A}{2}\left(\frac{\eta}{\eta_t} - 1\right)\frac{\eta}{\eta_t}} - \theta_t U_s$$

The term $\partial U_s/\partial(\xi/\eta_t)$ can be eliminated by equating it for the standard and nonstandard cases. Therefore,

$$\frac{\psi'}{\psi_t} = \frac{\eta}{\eta_t} +$$

$$\frac{A}{V_m}\left(\left[V_m\left(\frac{\psi}{\psi_t} - \frac{\eta}{\eta_t}\right)\right]_s + \frac{\eta}{\eta_t}\left(\frac{\eta}{\eta_t} - 1\right)\left\{\frac{U_s}{2}\left[\theta_t - (\theta_t)_s\right] + (R-R_s)(M_T\theta_t)_s\right\}\right) \tag{B16}$$

Equation (B16) is the correlation equation for the stream-function ratio.

1147

APPENDIX C

CORRELATION EQUATION FOR IMPELLER SLIP FACTOR

The impeller slip factor is defined as the ratio of the average absolute tangential velocity of the fluid leaving the impeller tip to the tip speed of the impeller. This definition results in the following equation (reference 1):

$$\mu = 1 + \frac{U_m}{M_T} \tag{C1}$$

Also, from equations (B1) and (B2)

$$\frac{U_m}{M_T} = \left(\frac{U_m}{M_T}\right)_s \frac{\theta_t}{(\theta_t)_s}$$

which, from equation (C1), becomes

$$\mu' - 1 = (\mu_s - 1) \frac{\theta_t}{(\theta_t)_s}$$

or

$$\mu' = 1 - (1 - \mu_s) \frac{\theta_t}{(\theta_t)_s} \tag{C2}$$

Equation (C2) is the correlation equation for the slip factor.

REFERENCES

1. Stanitz, John D.: Two-Dimensional Compressible Flow in Conical Mixed-Flow Compressors. NACA TN 1744, 1948.

2. Emmons, Howard W.: The Numerical Solution of Compressible Fluid Flow Problems. NACA TN 932, 1944.

3. Bickley, W. G.: Formulae for Numerical Differentiation. The Math. Gazette (London), vol. 25, pp. 19-27, 1941.

TABLE I - STREAM-FUNCTION RATIO ψ/ψ_t FOR STANDARD SOLUTION

[Conditions for standard example: $(\varphi)_s = 0.5$; $(M_T)_s = 1.5$; $(m)_s = -1.0$; $(\theta_t)_s = 0.20944$ radians; $(\gamma)_s = 1.4$]

$(V_m)_s$	R_s	ξ/η_t	η/η_t (equals θ/θ_t)										
			0	0.1	0.2	0.3	0.4	0.5	0.6	0.7	0.8	0.9	1.0
0.3168	0.70	-1.7030	0	0.040	0.095	0.165	0.244	0.341	0.451	0.570	0.702	0.848	1.000
.2941	.75	-1.3736	0	.031	.078	.143	.220	.316	.427	.549	.686	.840	1.000
.2735	.80	-1.0654	0	.022	.061	.120	.197	.291	.401	.529	.671	.831	1.000
.2536	.85	- .7760	0	.014	.047	.101	.177	.270	.383	.509	.655	.824	1.000
.2348	.90	- .5031	0	.011	.042	.097	.171	.265	.377	.503	.650	.819	1.000
.2275	.92	- .3981	0	.012	.046	.102	.177	.270	.382	.506	.651	.816	1.000
.2202	.94	- .2954	0	.016	.054	.113	.189	.283	.392	.517	.660	.820	1.000
.2133	.96	- .1949	0	.023	.069	.132	.212	.305	.413	.536	.675	.828	1.000
.2100	.97	- .1454	0	.029	.080	.146	.228	.321	.429	.550	.684	.832	1.000
.2067	.98	- .0965	0	.038	.093	.163	.247	.341	.447	.566	.697	.839	1.000
.2034	.99	- .0480	0	.048	.111	.185	.270	.366	.472	.586	.713	.850	1.000
.2002	1.00	0	0	.062	.133	.210	.297	.393	.499	.611	.734	.862	1.000

TABLE II - RADIAL-VELOCITY RATIO V FOR STANDARD SOLUTION

[Conditions for standard example: $(\varphi)_s = 0.5$; $(M_T)_s = 1.5$; $(m)_s = -1.0$; $(\theta_t)_s = 0.20944$ radians; $(\gamma)_s = 1.4$]

$(V_m)_s$	R_s	ξ/η_t	η/η_t (equals θ/θ_t)										
			0	0.1	0.2	0.3	0.4	0.5	0.6	0.7	0.8	0.9	1.0
0.3168	0.70	-1.7030	0.103	0.146	0.190	0.234	0.278	0.323	0.368	0.412	0.456	0.501	0.549
.2941	.75	-1.3736	.085	.112	.159	.206	.253	.301	.348	.396	.443	.492	.543
.2735	.80	-1.0654	.033	.082	.132	.181	.230	.280	.329	.378	.428	.479	.533
.2536	.85	- .7760	.008	.059	.110	.160	.210	.259	.309	.357	.408	.460	.515
.2348	.90	- .5031	-.001	.049	.099	.148	.194	.239	.285	.330	.378	.430	.483
.2275	.92	- .3981	.002	.051	.100	.146	.189	.231	.273	.316	.363	.413	.463
.2202	.94	- .2954	.010	.058	.105	.148	.186	.224	.261	.299	.342	.390	.438
.2133	.96	- .1949	.025	.072	.115	.151	.184	.216	.248	.280	.316	.360	.407
.2100	.97	- .1454	.037	.082	.122	.155	.184	.213	.241	.270	.301	.342	.388
.2067	.98	- .0965	.055	.095	.131	.158	.184	.209	.234	.259	.286	.321	.362
.2034	.99	- .0480	.091	.115	.139	.161	.184	.205	.227	.249	.271	.293	.316
.2002	1.00	0	.199	.131	.148	.166	.184	.202	.220	.238	.254	.271	.199

1147

1147

TABLE III - RELATIVE TANGENTIAL-VELOCITY RATIO U FOR STANDARD SOLUTION

[Conditions for standard example: $(M_T)_s = 1.5$; $(\theta_t)_s = 0.20944$ radians]

R_s	ξ/η_t	η/η_t (equals θ/θ_t)										
		0	0.1	0.2	0.3	0.4	0.5	0.6	0.7	0.8	0.9	1.0
0.70	-1.7030	0	0.008	0.015	0.020	0.023	0.024	0.023	0.020	0.015	0.008	0
.75	-1.3736	0	.008	.015	.020	.023	.024	.023	.020	.015	.008	0
.80	-1.0654	0	.008	.014	.018	.021	.022	.021	.019	.015	.008	0
.85	- .7760	0	.005	.009	.011	.012	.013	.013	.012	.010	.008	0
.90	- .5031	0	- .002	- .004	- .007	- .008	- .008	- .007	- .005	- .003	- .001	0
.92	- .3981	0	- .007	- .013	- .018	- .021	- .022	- .021	- .016	- .011	- .005	0
.94	- .2954	0	- .013	- .024	- .033	- .038	- .039	- .037	- .031	- .022	- .012	0
.96	- .1949	0	- .023	- .041	- .054	- .061	- .063	- .060	- .052	- .039	- .021	0
.97	- .1454	0	- .030	- .053	- .068	- .076	- .077	- .074	- .066	- .050	- .029	0
.98	- .0965	0	- .040	- .067	- .083	- .091	- .094	- .091	- .081	- .065	- .039	0
.99	- .0480	0	- .053	- .083	- .100	- .109	- .112	- .108	- .099	- .082	- .052	0
1.00	0	0	- .072	- .102	- .119	- .128	- .131	- .127	- .118	- .100	- .070	0

1147

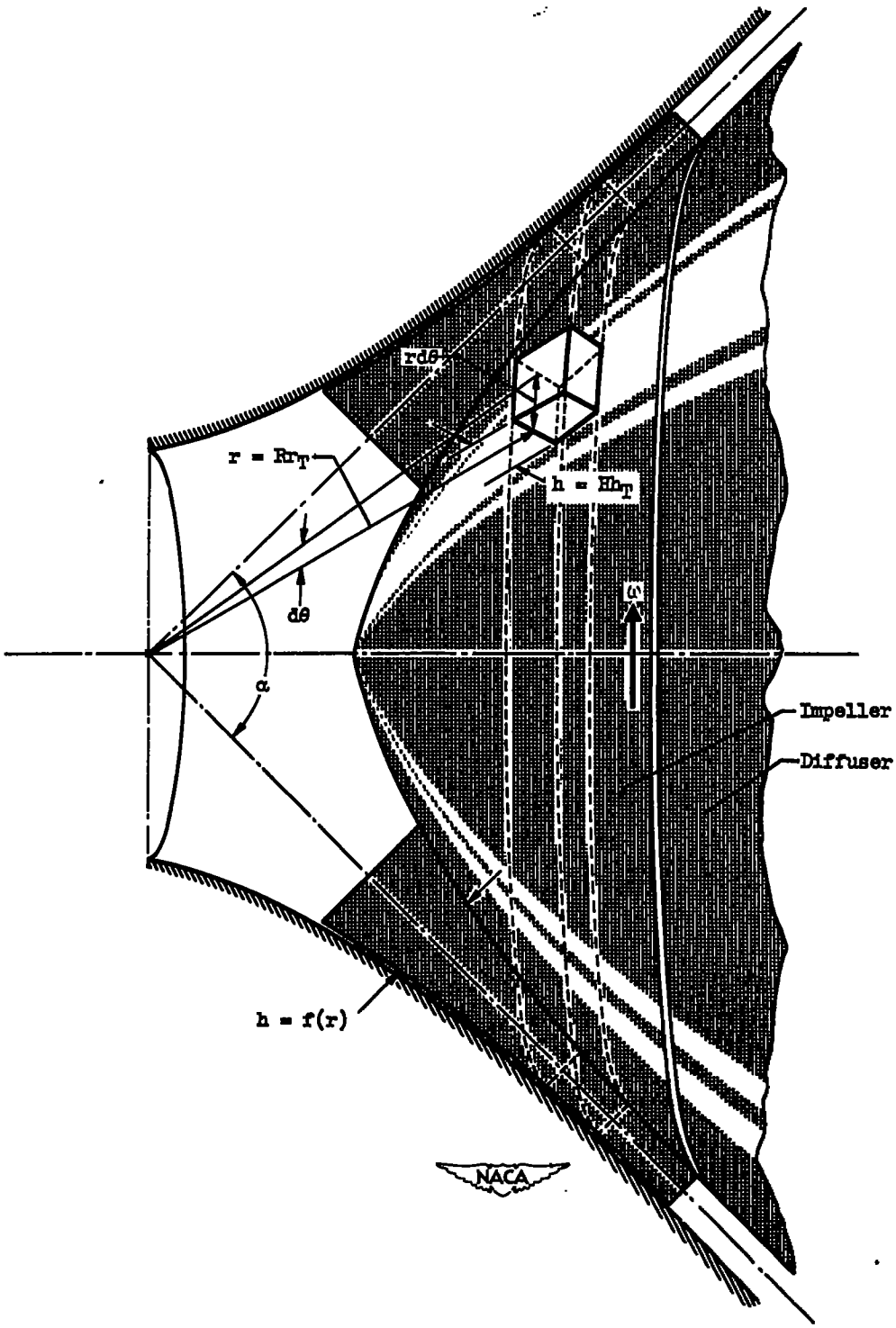

Figure 1. - Fluid particle on rotating coordinate system of impeller. Center line of flow passage generates right circular cone with cone angle α.

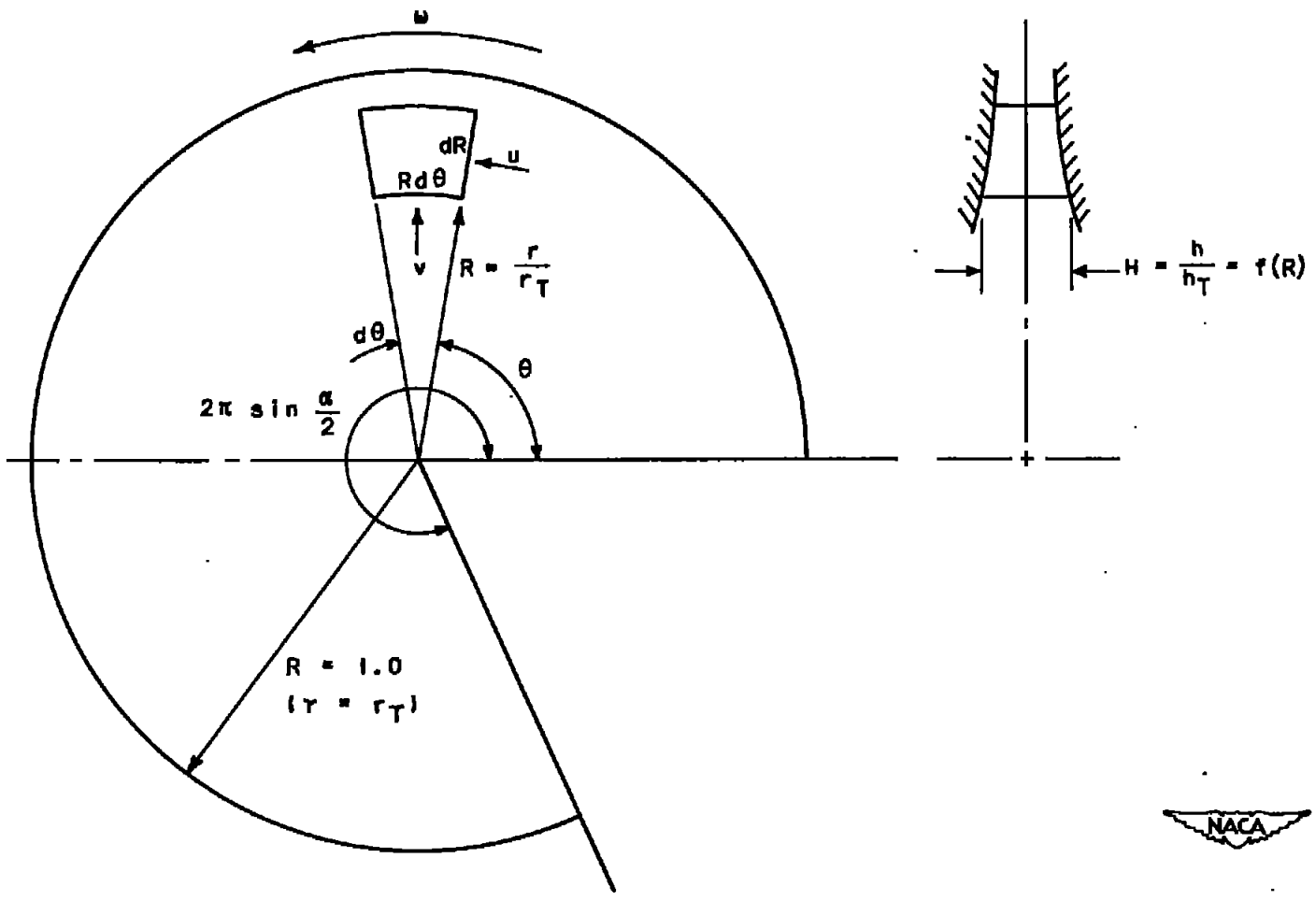

Figure 2. - Fluid particle on developed view of conic surface. R, θ, and H, dimensionless coordinates relative to impeller; u and v, tangential and radial components of velocity relative to impeller, respectively.

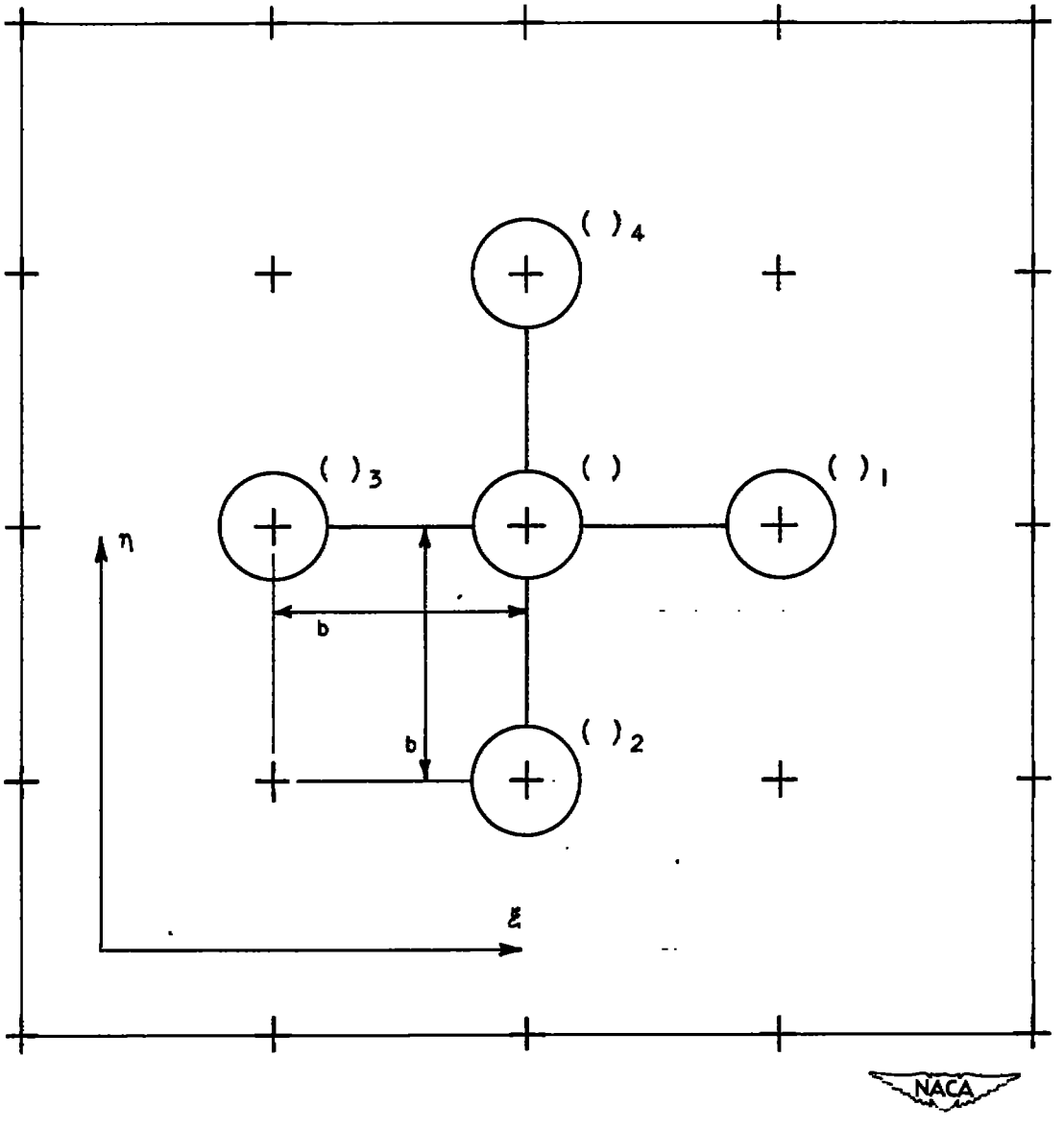

Figure 3. - Sample grid showing grid spacing b and numerical subscript convention for adjacent grid points.

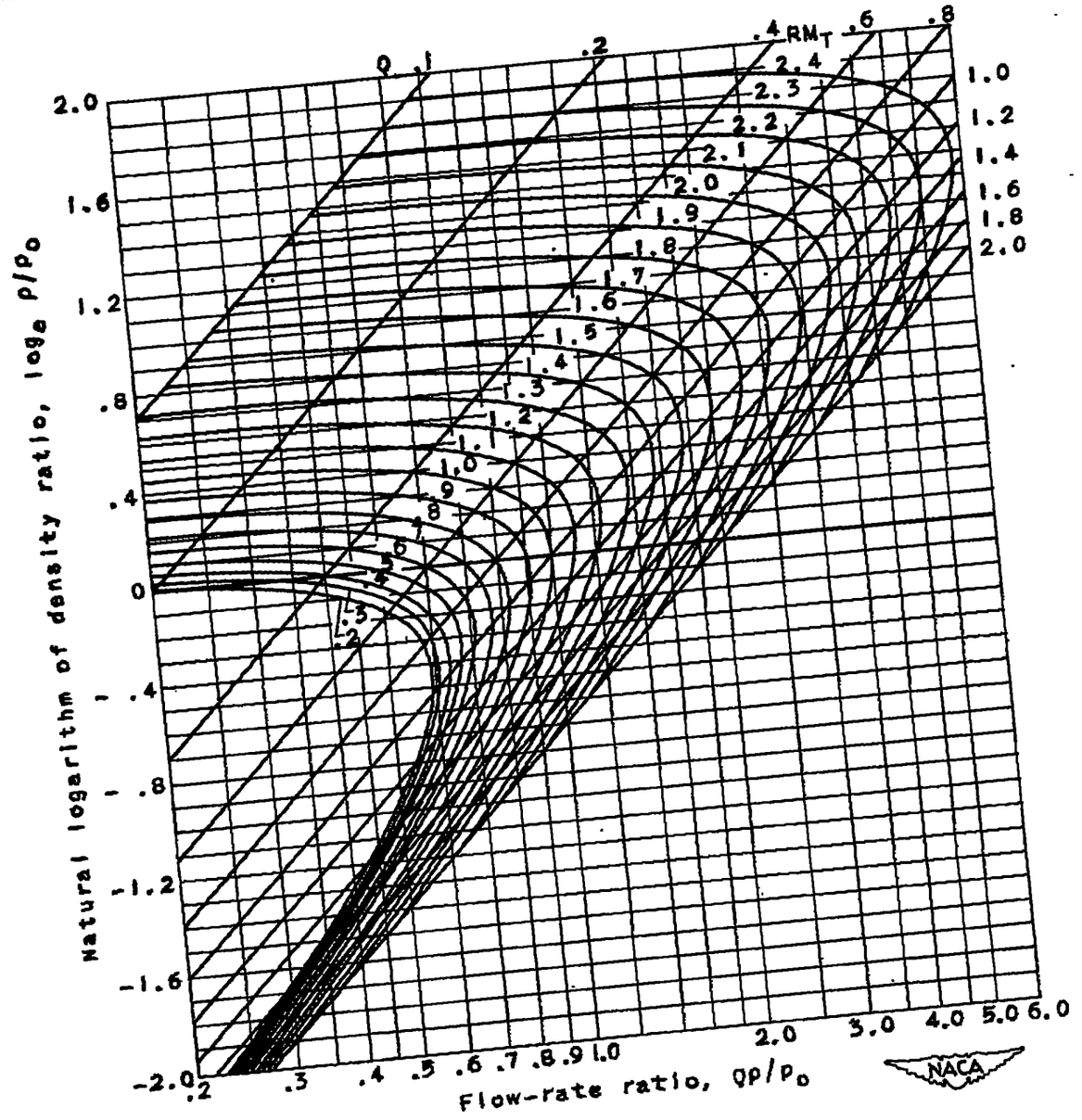

Figure 4. - Natural logarithm of density ratio $\log_e \rho/\rho_o$ as function of flow-rate ratio $Q\rho/\rho_o$ for various values of RM_T. Equation (12); ratio of specific heats γ, 1.4.

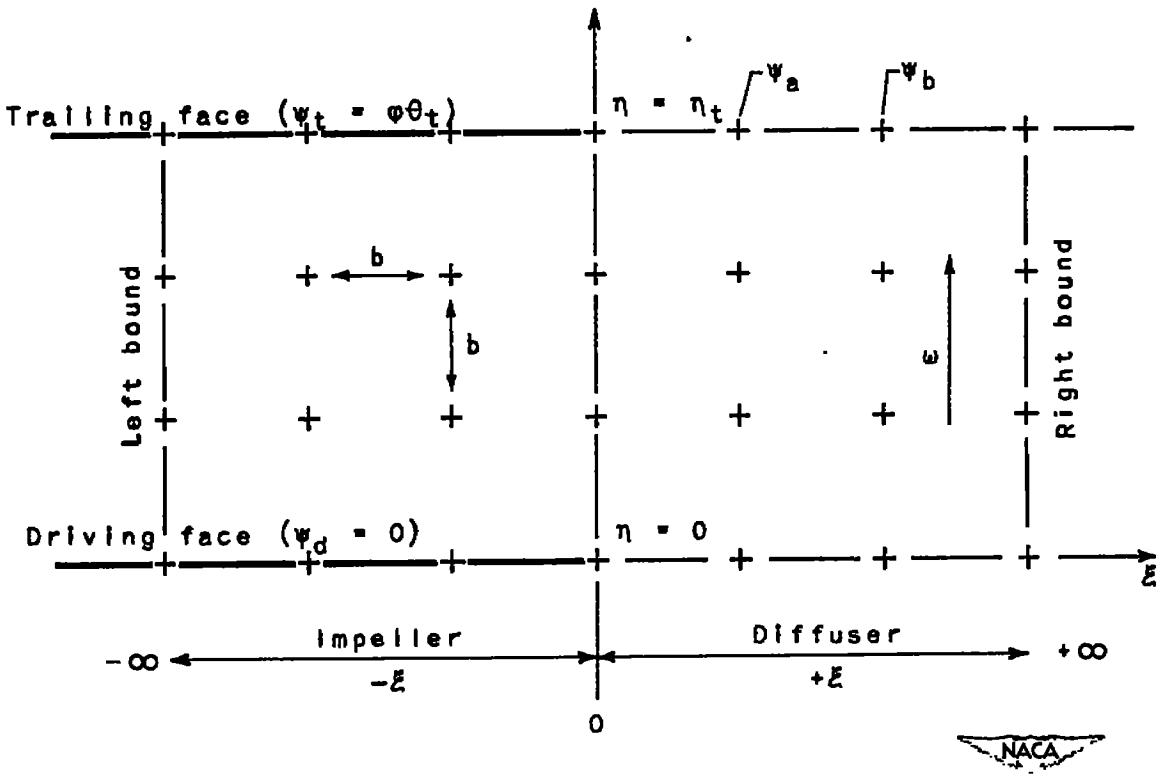

Figure 5. - Relaxation grid in transformed coordinates.

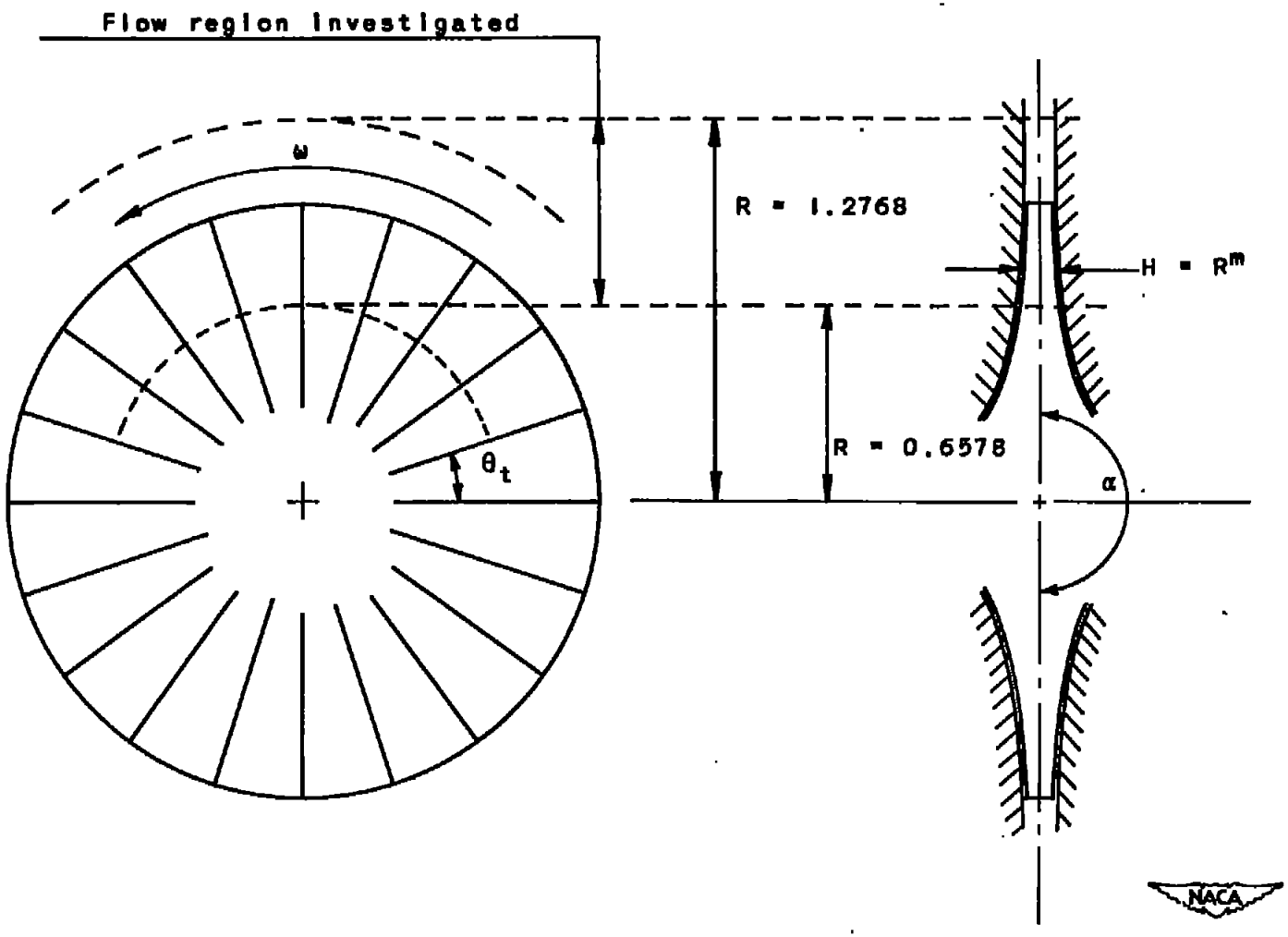

Figure 6. - Compressor-design characteristics for numerical examples.

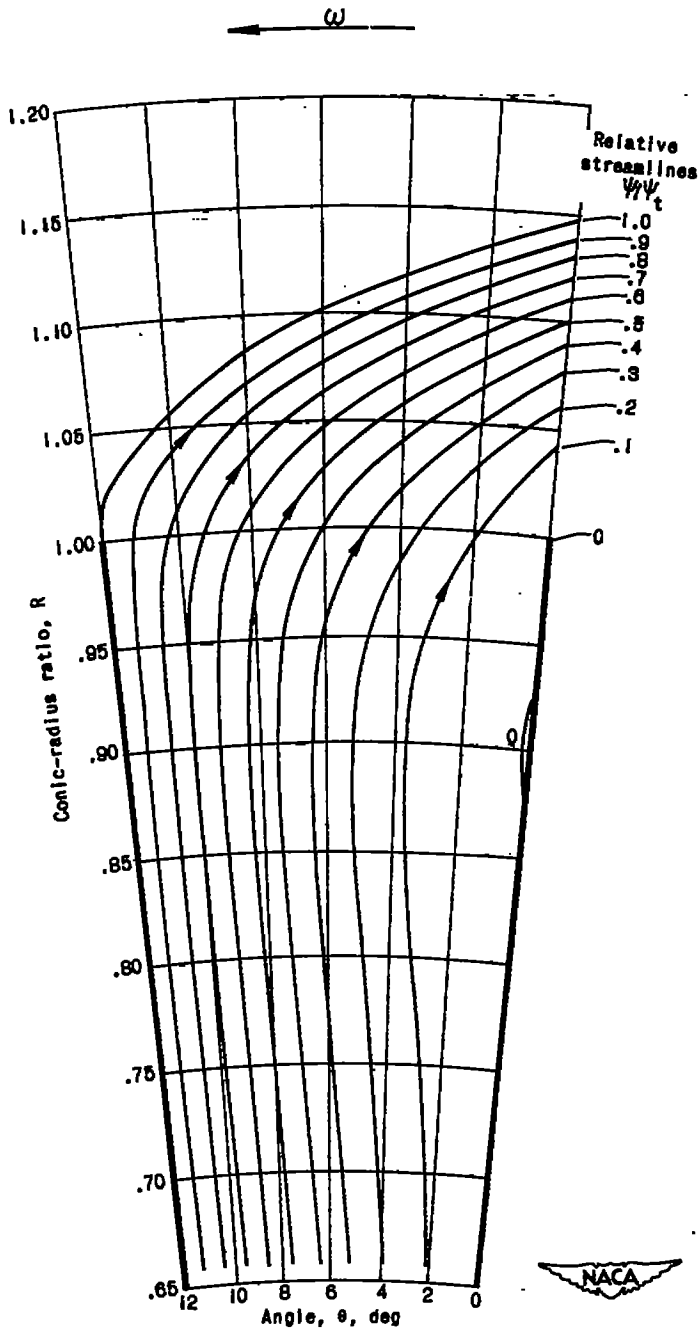

(a) Standard example: flow coefficient φ, 0.5; impeller-tip Mach number M_T, 1.5; constant flow area (m, 1.0); included passage angle θ_t, 12°; compressible flow (γ, 1.4). (An extra copy of this figure is enclosed to enable direct comparison with streamlines of nonstandard examples.)

Figure 7. - Relative streamlines for flow through centrifugal compressor with straight blades. Streamline designation indicates percentage of flow through passage between streamline and driving face of blade (right side of passage).

1147

1147

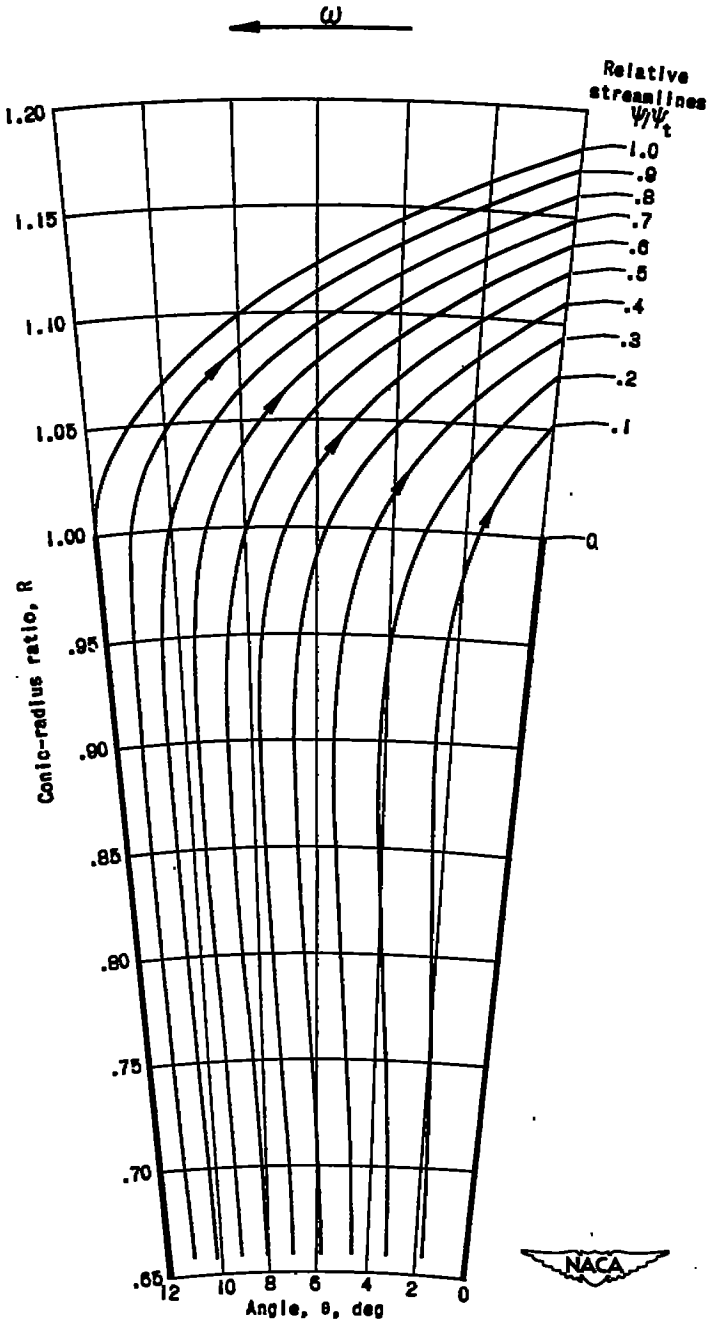

(b) Example 1: flow coefficient φ, 0.7; other parameters same as standard example.

Figure 7. - Continued. Relative streamlines for flow through centrifugal compressor with straight blades. Streamline designation indicates percentage of flow through passage between streamline and driving face of blade (right side of passage).

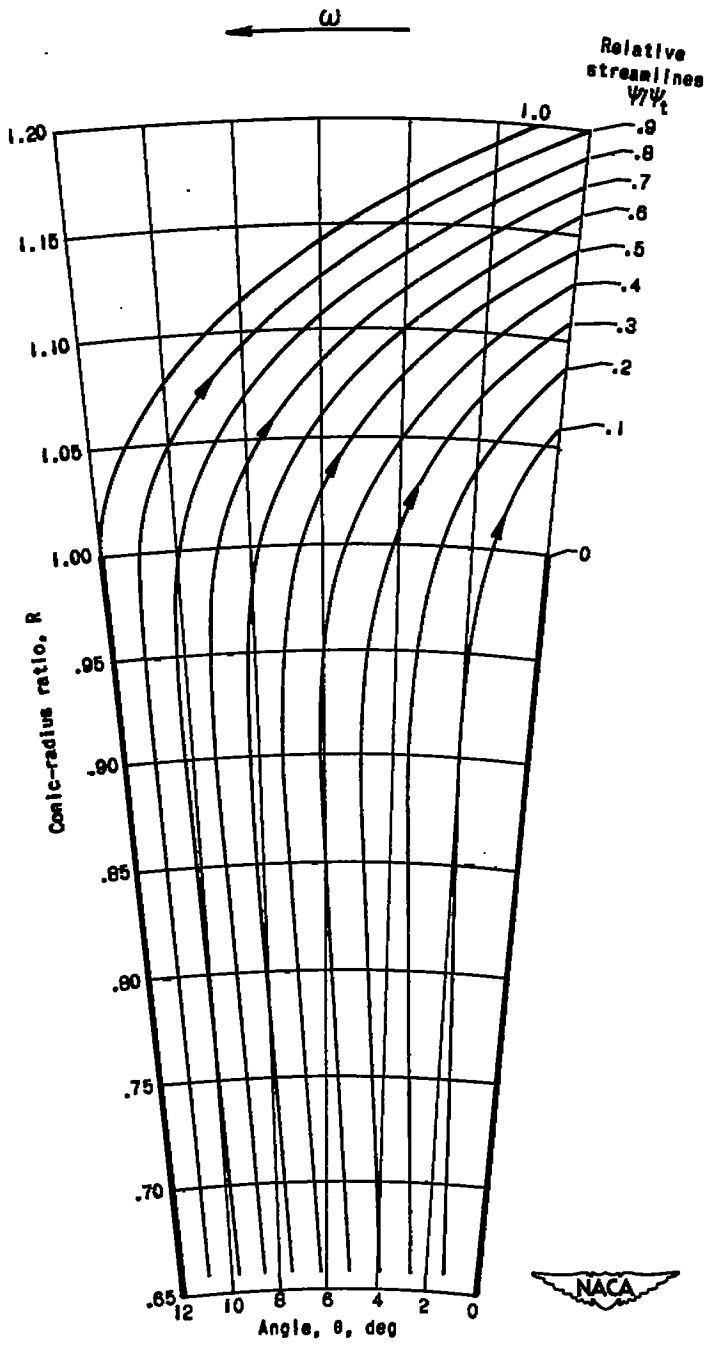

(c) Example 2: flow coefficient φ, 0.9; other parameters same as standard example.

Figure 7. - Continued. Relative streamlines for flow through centrifugal compressor with straight blades. Streamline designation indicates percentage of flow through passage between streamline and driving face of blade (right side of passage).

1147

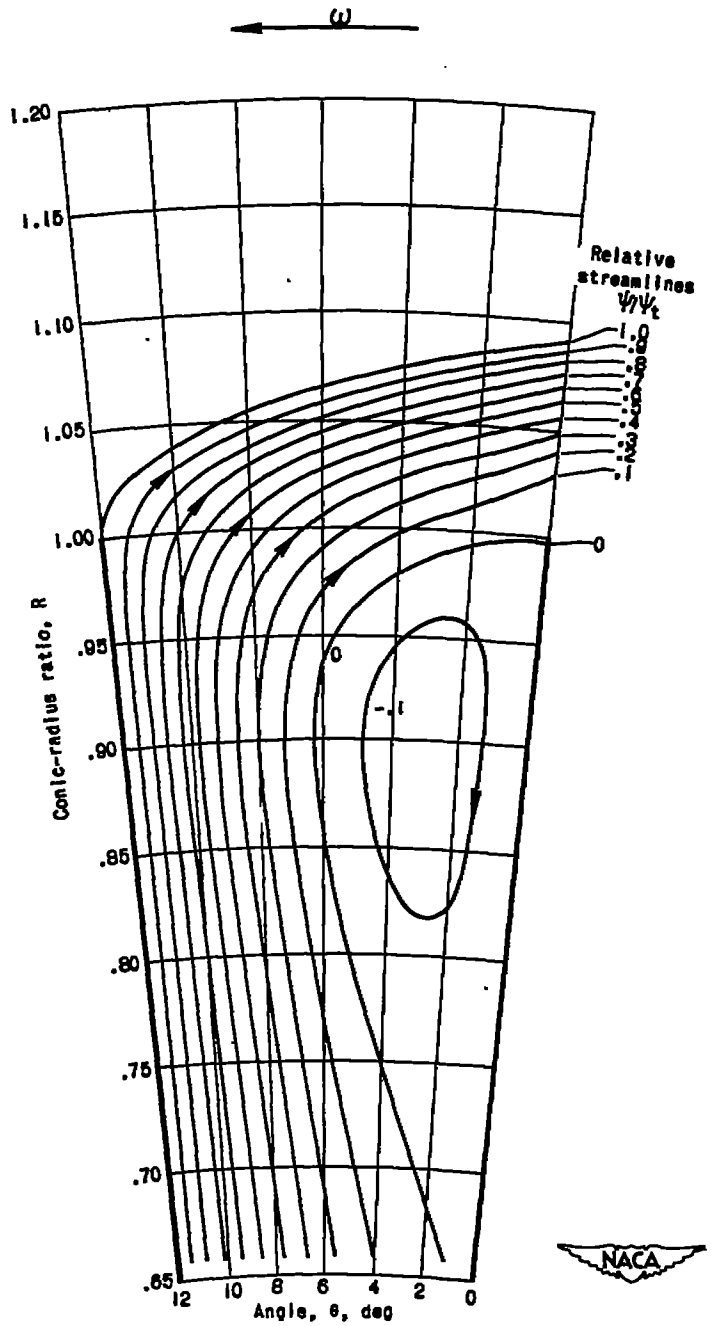

(d) Example 3: Impeller-tip Mach number M_T, 2.0; other parameters same as standard example.

Figure 7. - Continued. Relative streamlines for flow through centrifugal compressor with straight blades. Streamline designation indicates percentage of flow through passage between streamline and driving face of blade (right side of passage).

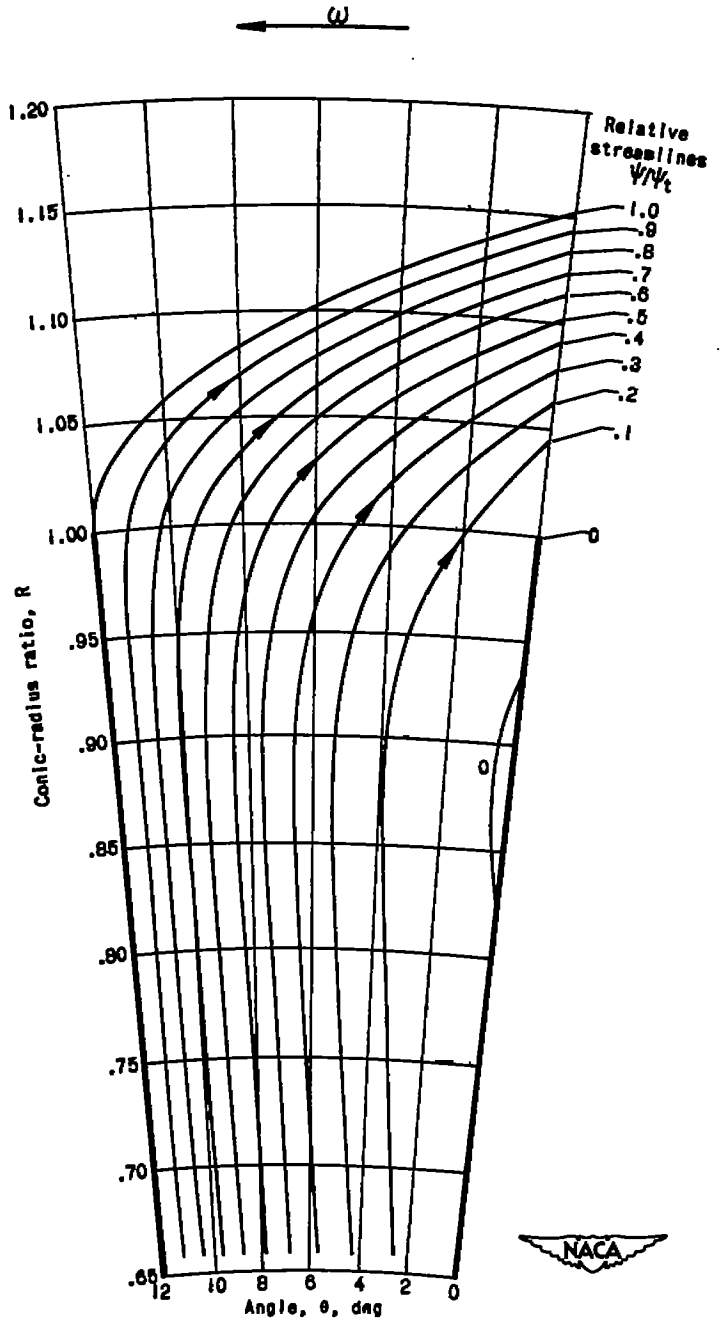

(e) Example 4: varying flow area (m, -1.4); other parameters same as standard example.

Figure 7. - Continued. Relative streamlines for flow through centrifugal compressor with straight blades. Streamline designation indicates percentage of flow through passage between streamline and driving face of blade (right side of passage).

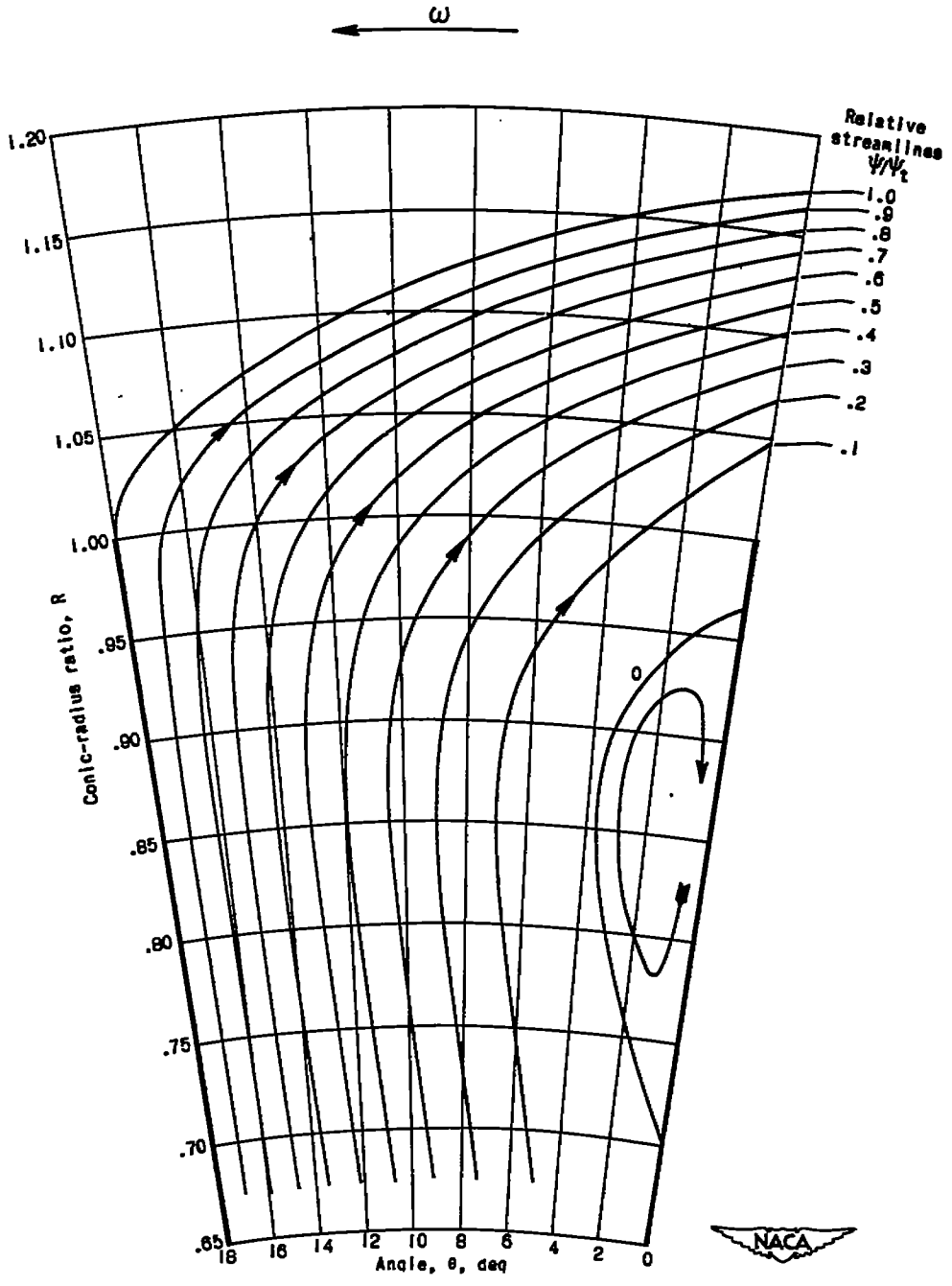

(f) Example 5: included passage angle θ_t, 18°; other parameters same as standard example.

Figure 7. - Continued. Relative streamlines for flow through centrifugal compressor with straight blades. Streamline designation indicates percentage of flow through passage between streamline and driving face of blade (right side of passage).

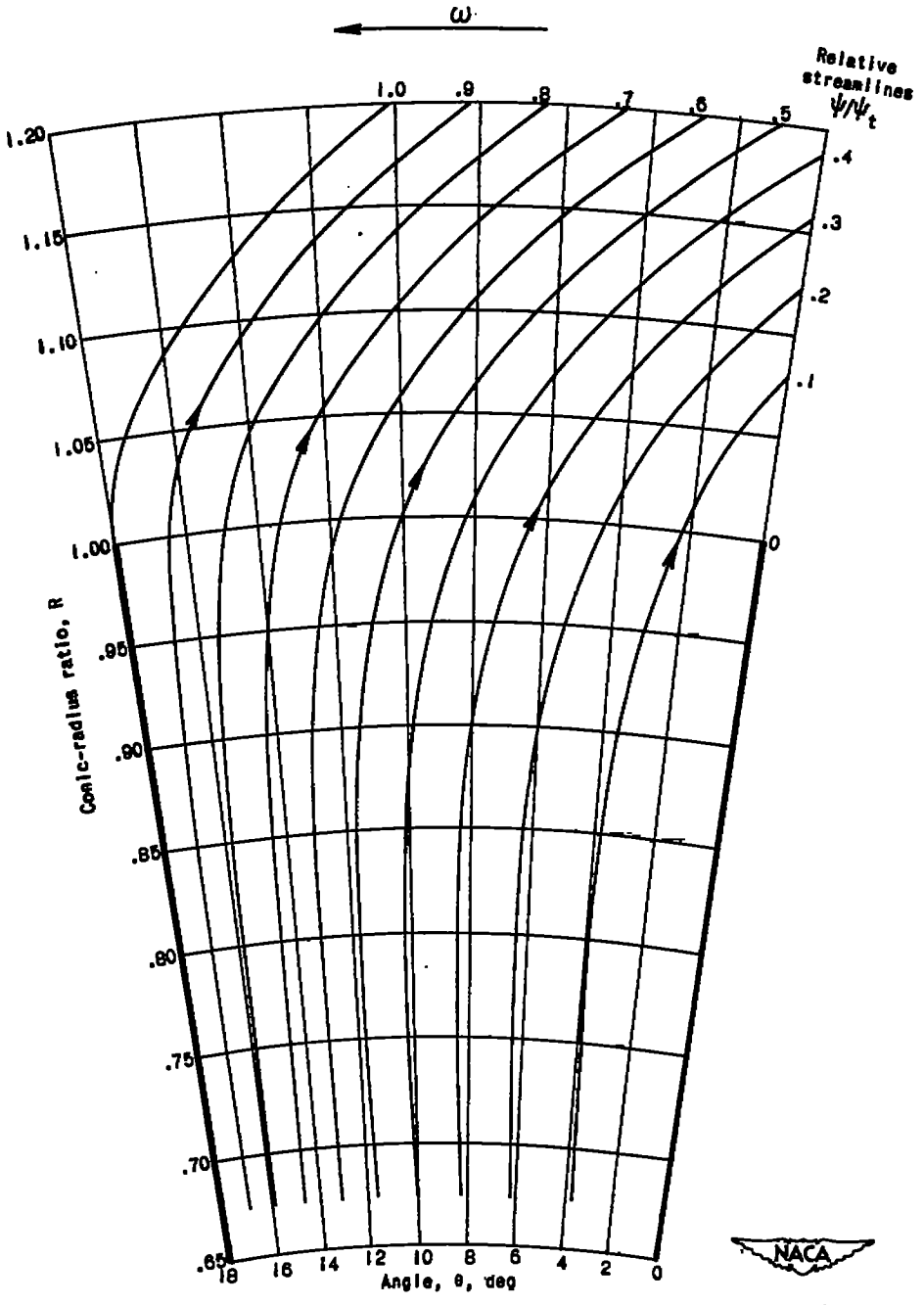

(g) Example 6: Incompressible fluid; other parameters same as example 5 (fig. 7(f)). Note that φ and M_T are based upon same constant c_0, the magnitude of which is equal to speed of sound at inlet conditions of example 5.)

Figure 7. - Concluded. Relative streamlines for flow through centrifugal compressor with straight blades. Streamline designation indicates percentage of flow through passage between streamline and driving face of blade (right side of passage).

1147

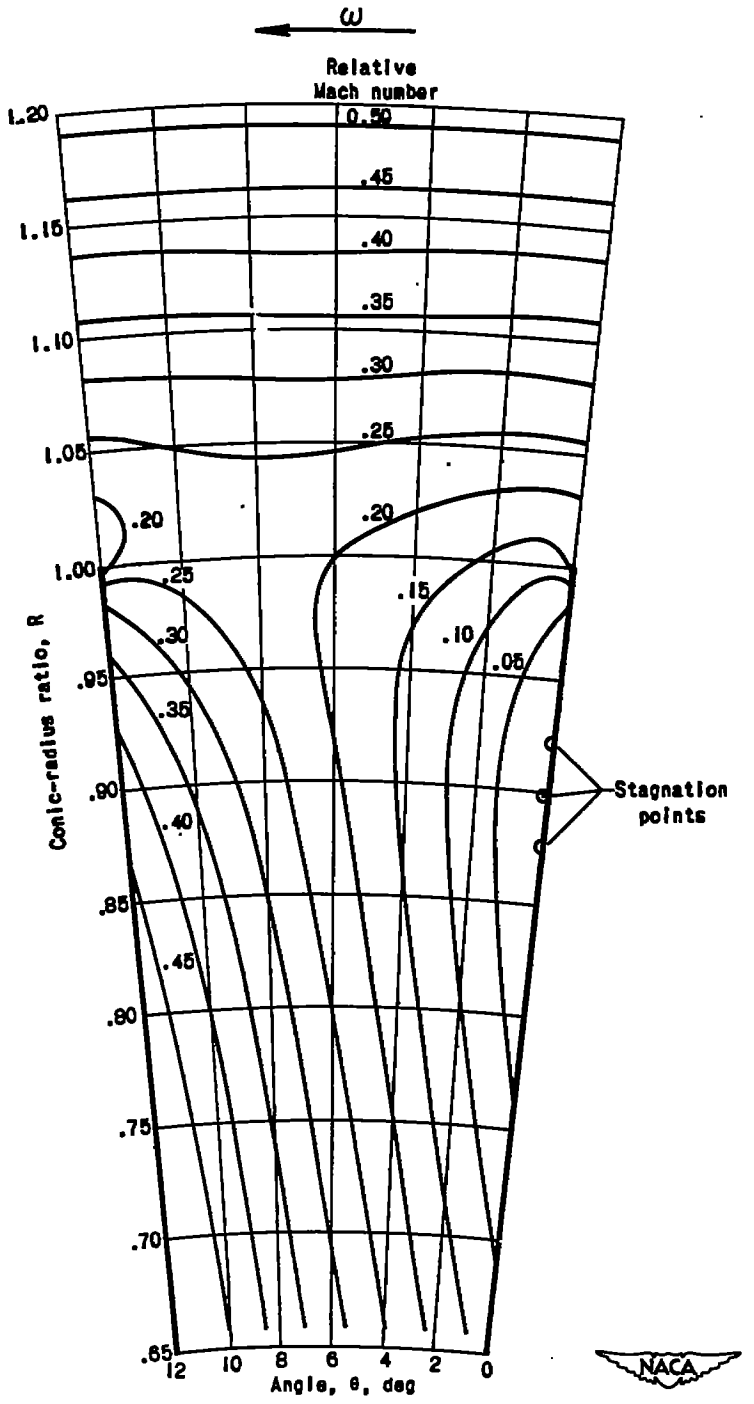

(a) Standard example: flow coefficient φ, 0.5; impeller-tip Mach number M_T, 1.5; constant flow area (m, -1.0); included passage angle θ_t, 12°; compressible flow (γ, 1.4). (An extra copy of this figure is enclosed to enable direct comparison with constant Mach number lines of nonstandard examples.)

Figure 8. - Lines of constant Mach number relative to impeller.

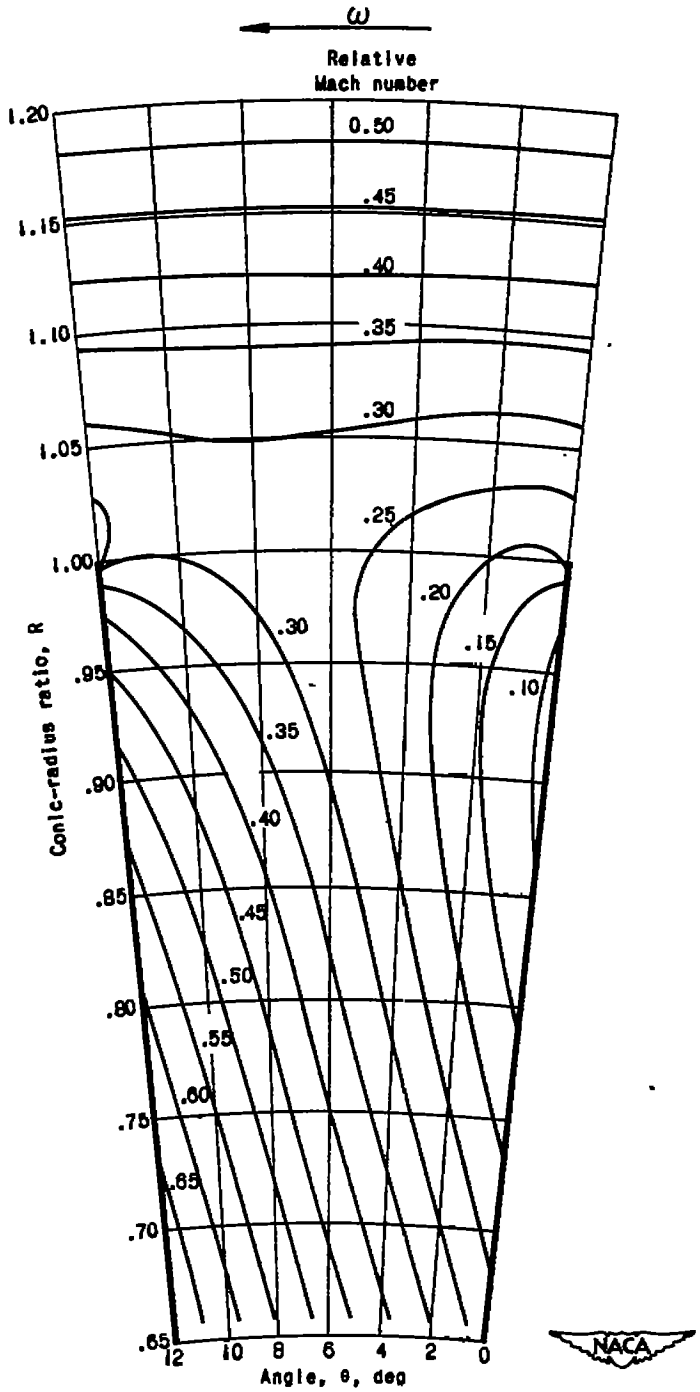

(b) Example I: flow coefficient φ, 0.7; other parameters same as standard example.

Figure 8. - Continued. Lines of constant Mach number relative to impeller.

1147

1147

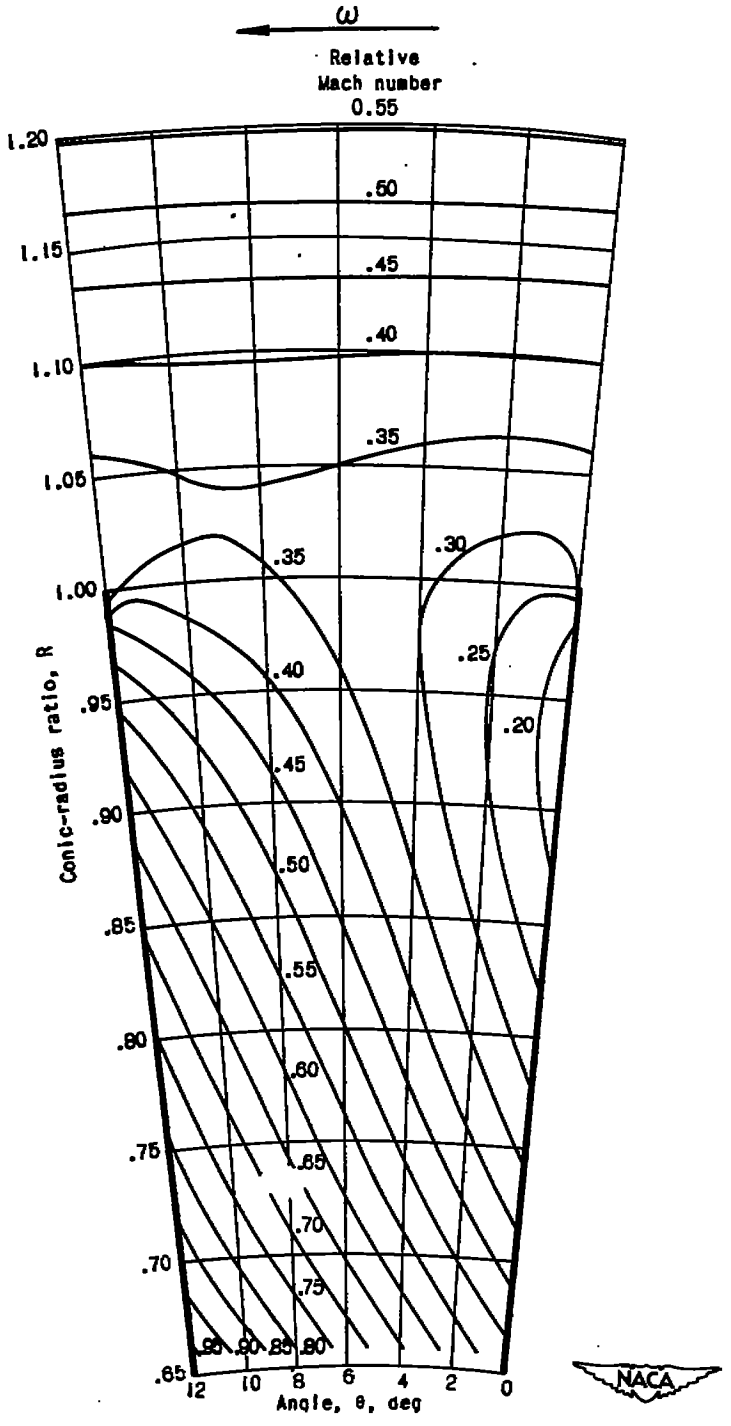

(c) Example 2: flow coefficient φ, 0.9; other parameters same as standard example.

Figure 8. - Continued. Lines of constant Mach number relative to impeller.

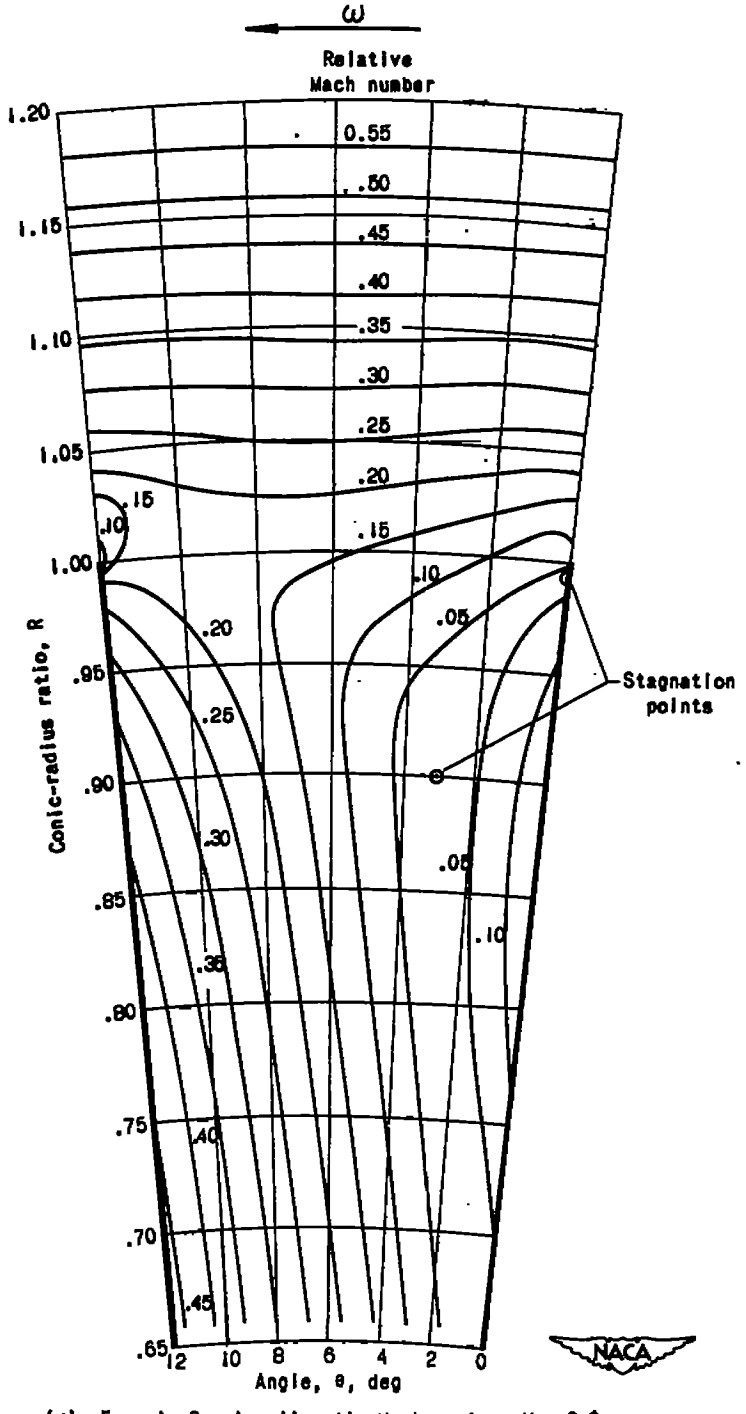

(d) Example 3: Impeller-tip Mach number M_T, 2.0; other parameters same as standard example.

Figure 8. - Continued. Lines of constant Mach number relative to impeller.

1147

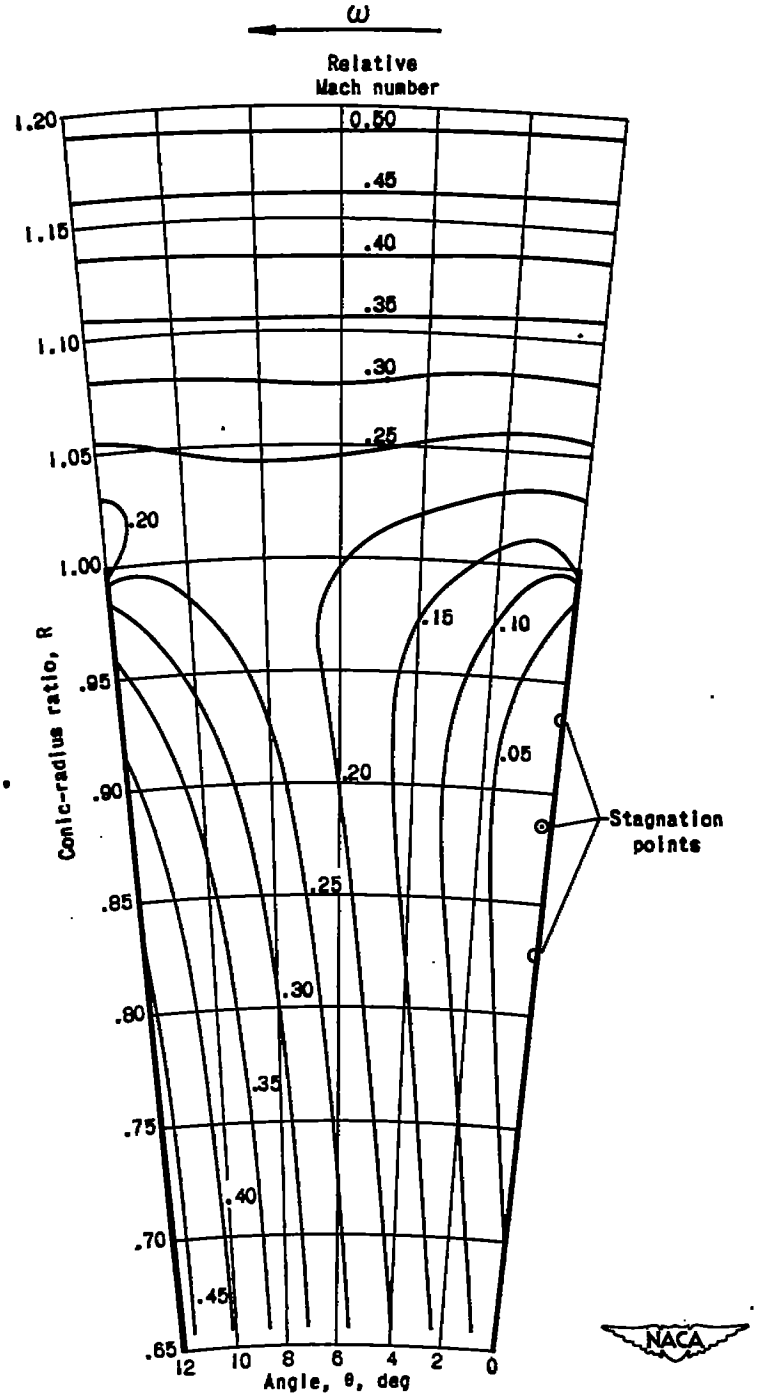

(e) Example 4: varying flow area (m, -1.4); other parameters same as standard example.

Figure 8. - Continued. Lines of constant Mach number relative to impeller.

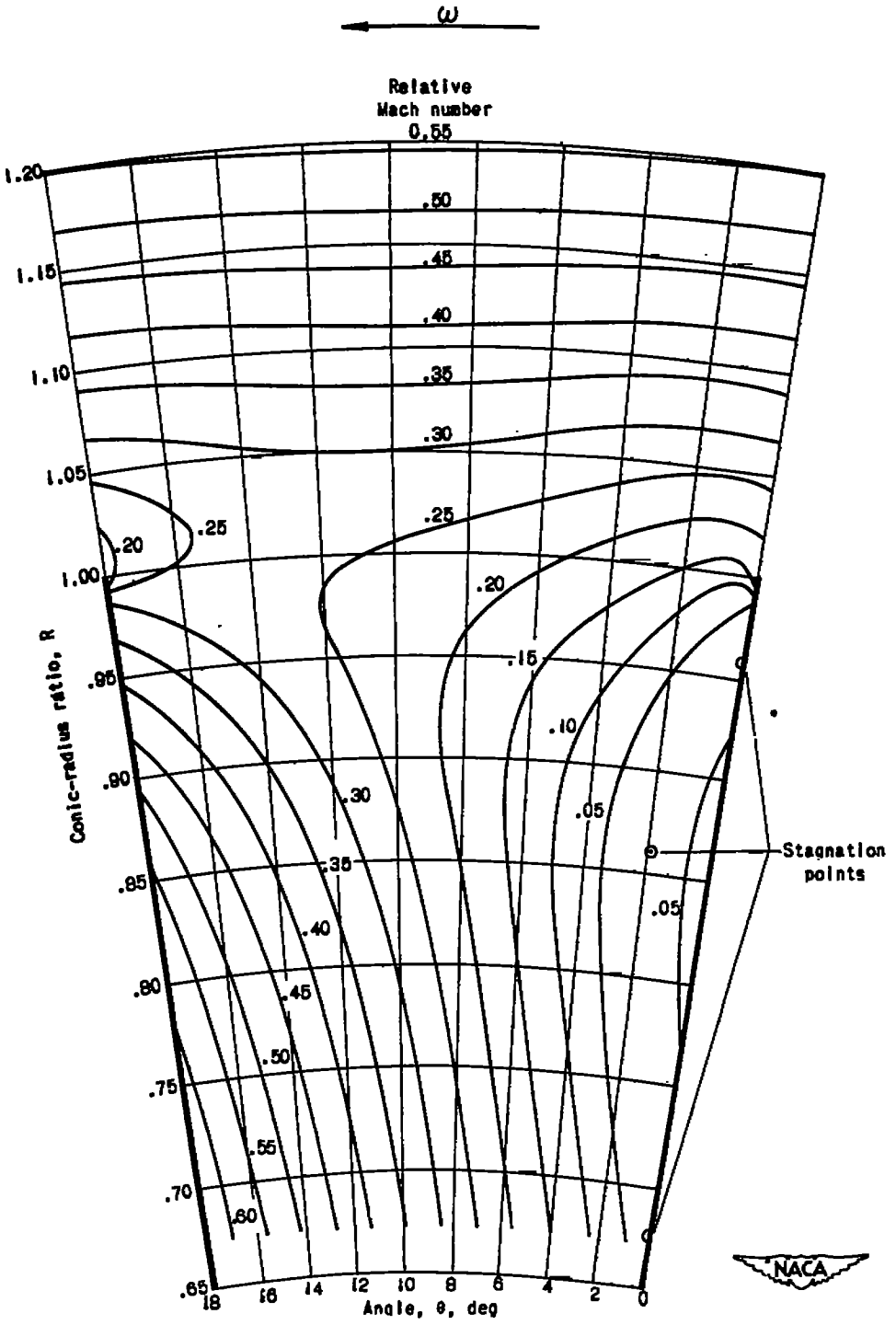

(f) Example 5: Included passage angle θ_t, 18°; other parameters same as standard example.

Figure 8. - Continued. Lines of constant Mach number relative to impeller.

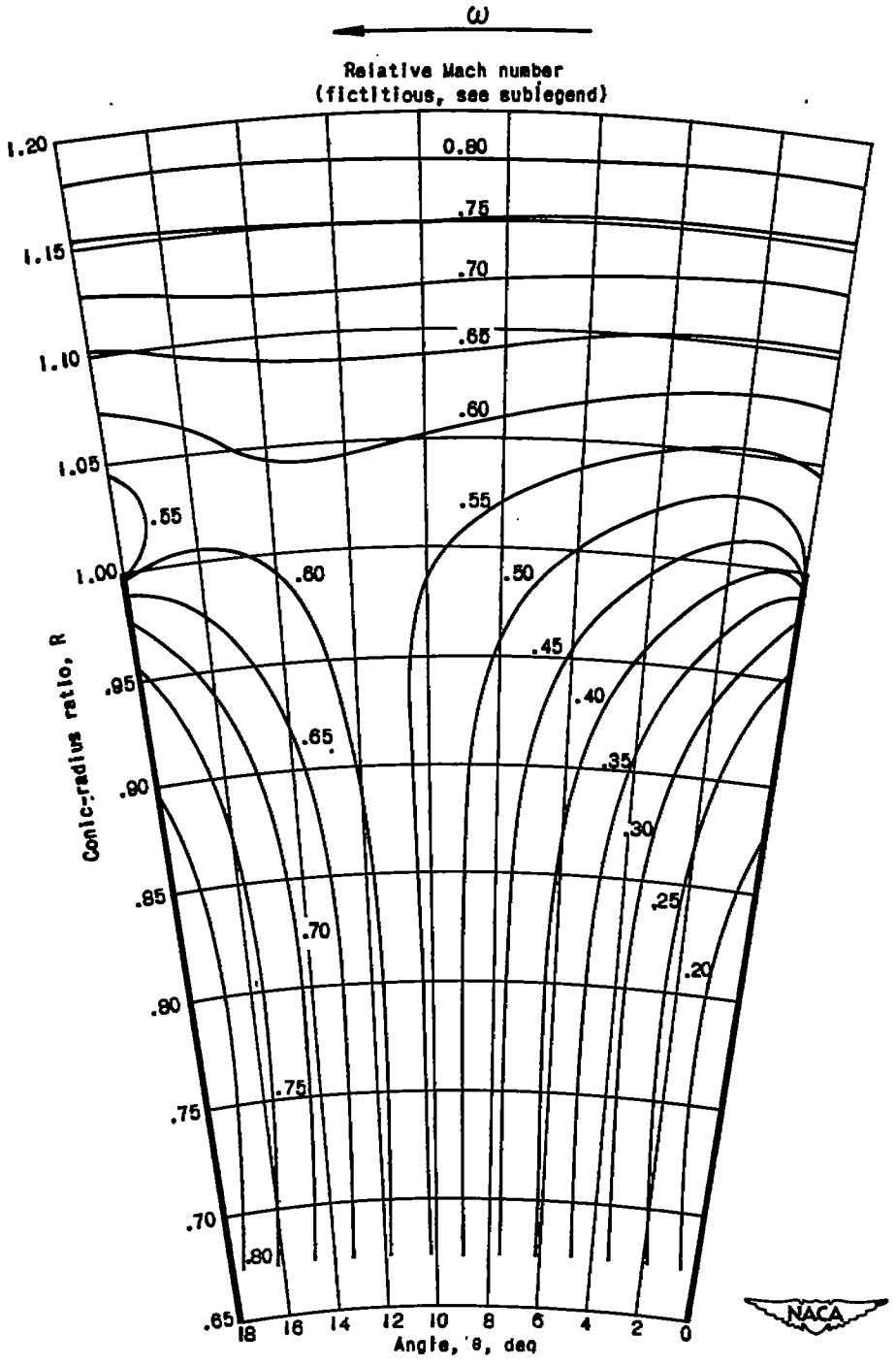

(g) Example 6: incompressible fluid; other parameters same as example 5 (fig. 8(f)). (Note that φ, and M_T are based upon same constant c_0, the magnitude of which is equal to speed of sound at inlet conditions of example 5. For incompressible fluids the relative Mach number becomes fictitious and is equal to relative velocity q divided by constant c_0.)

Figure 8. - Concluded. Lines of constant Mach number relative to impeller.

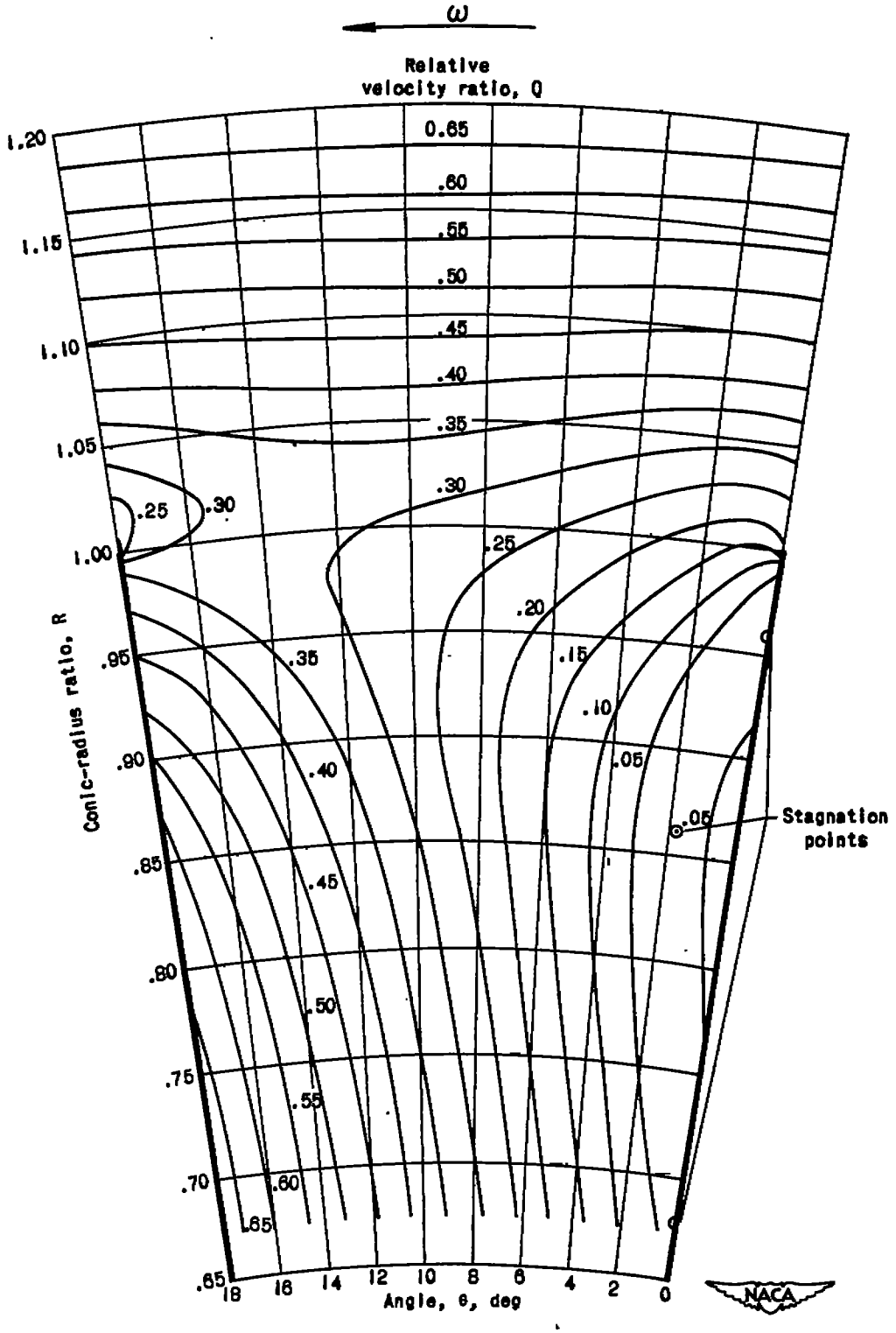

Figure 9. - Lines of constant velocity ratio relative to impeller. Example 5; flow coefficient φ, 0.5; impeller-tip Mach number M_T, 1.5; constant flow area (m,-1.0); included passage angle θ_t, 18°; compressible flow (γ, 1.4).

1147

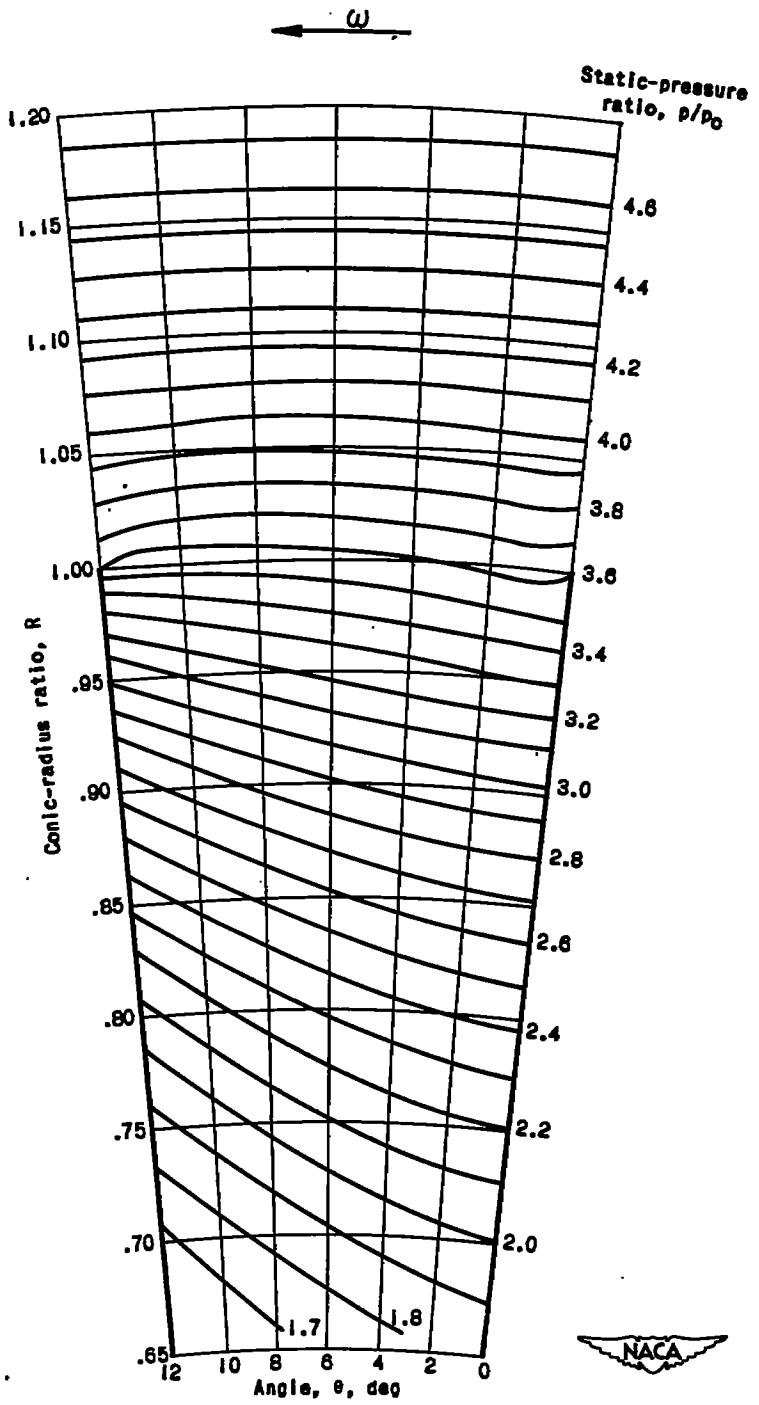

(a) Standard example: flow coefficient φ, 0.5; impeller-tip Mach number M_T, 1.5; constant flow area (m, -1.0); included passage angle θ_t, 12°; compressible flow (γ, 1.4). (An extra copy of this figure is enclosed to enable direct comparison with constant pressure-ratio lines of nonstandard examples.)

Figure 10. - Lines of constant static-pressure ratio.

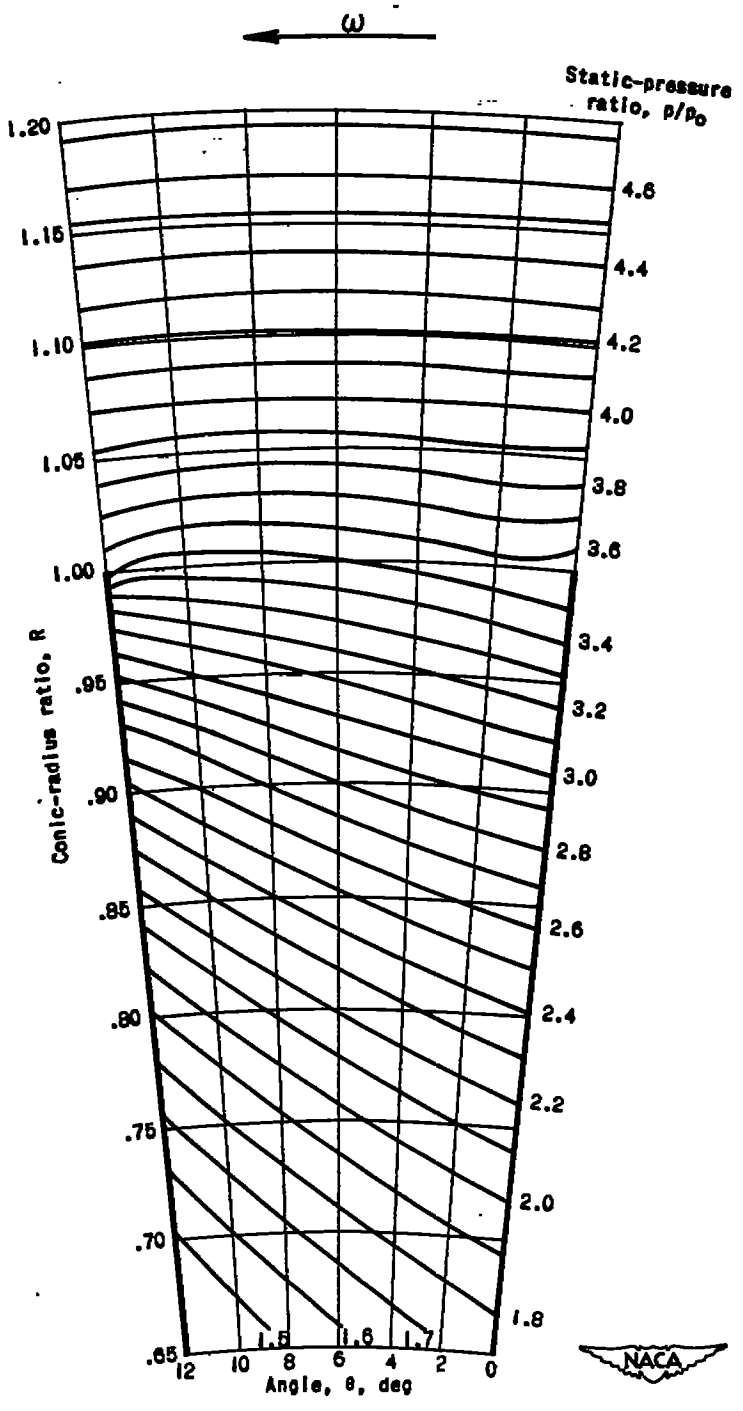

(b) Example 1: flow coefficient φ, 0.7; other parameters same as standard example.

Figure 10. - Continued. Lines of constant static-pressure ratio.

1147

1147

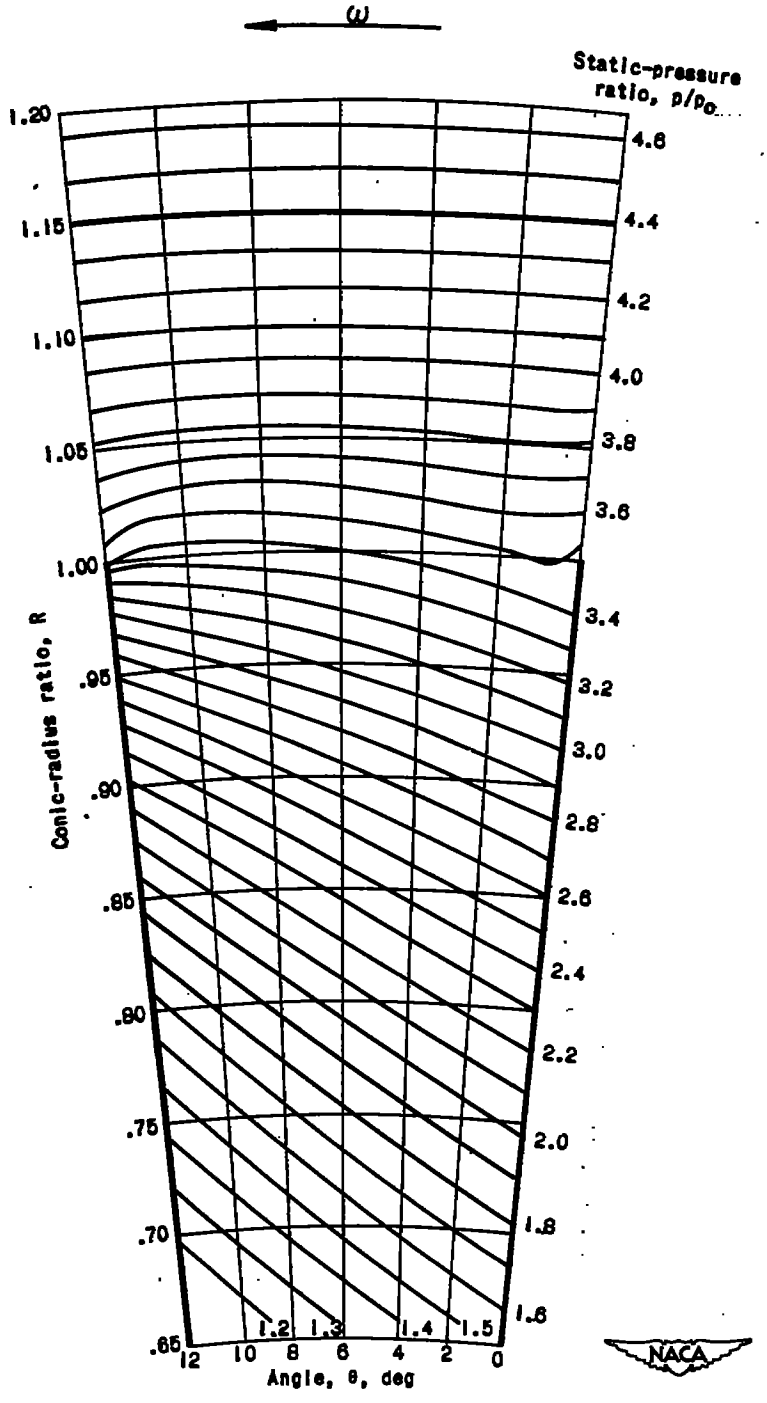

(c) Example 2: flow coefficient φ, 0.9; other parameters same as standard example.

Figure 10. - Continued. Lines of constant static-pressure ratio.

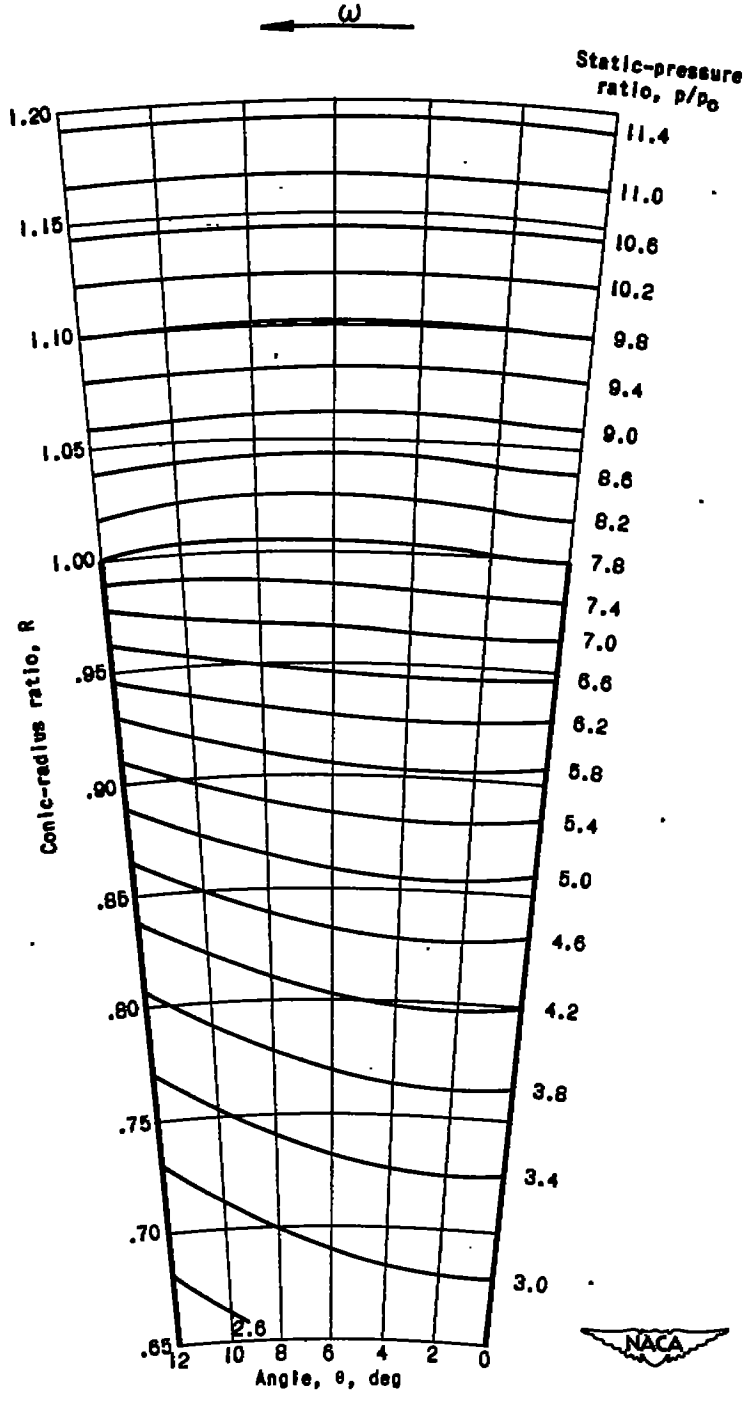

(d) Example 3: Impeller-tip Mach number M_T, 2.0; other parameters same as standard example.

Figure 10. - Continued. Lines of constant static-pressure ratio.

1147

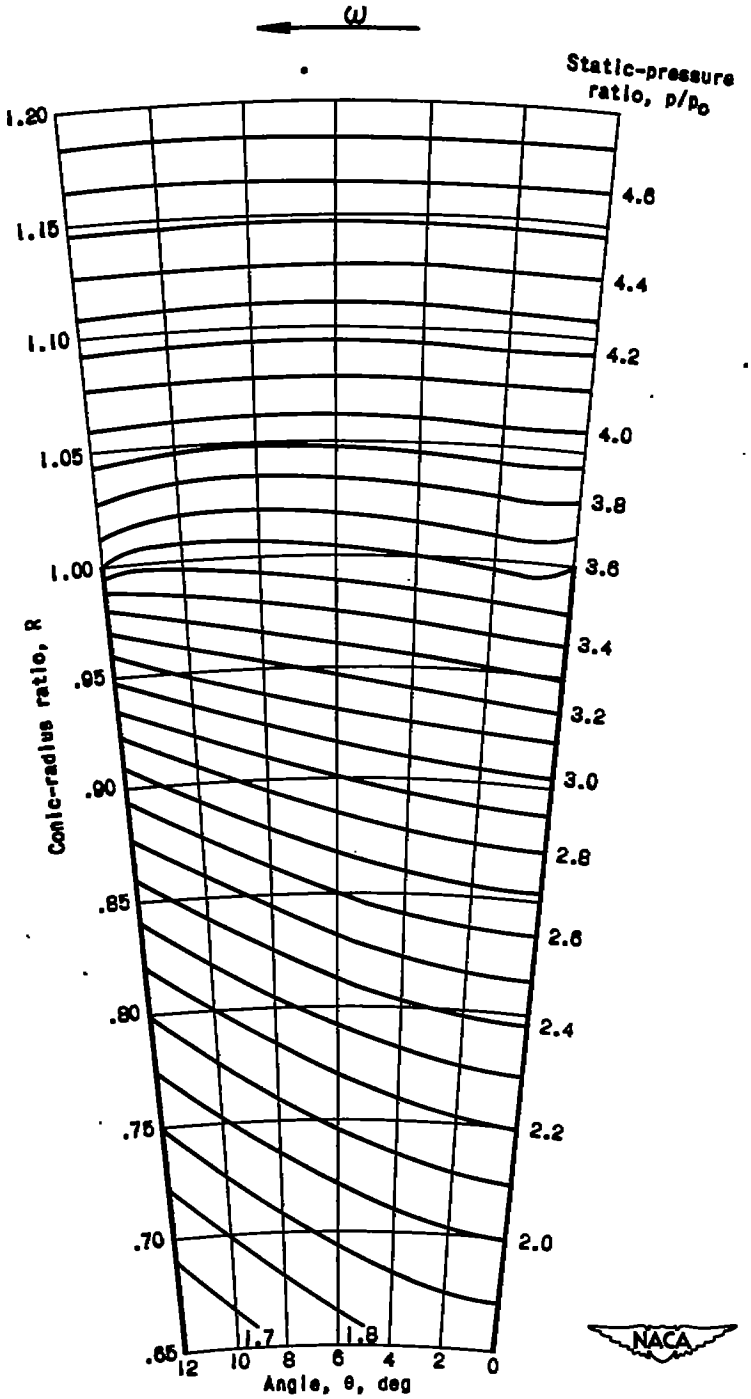

(e) Example 4: varying flow area (m, -1.4); other parameters same as standard example.

Figure 10. - Continued. Lines of constant static-pressure ratio.

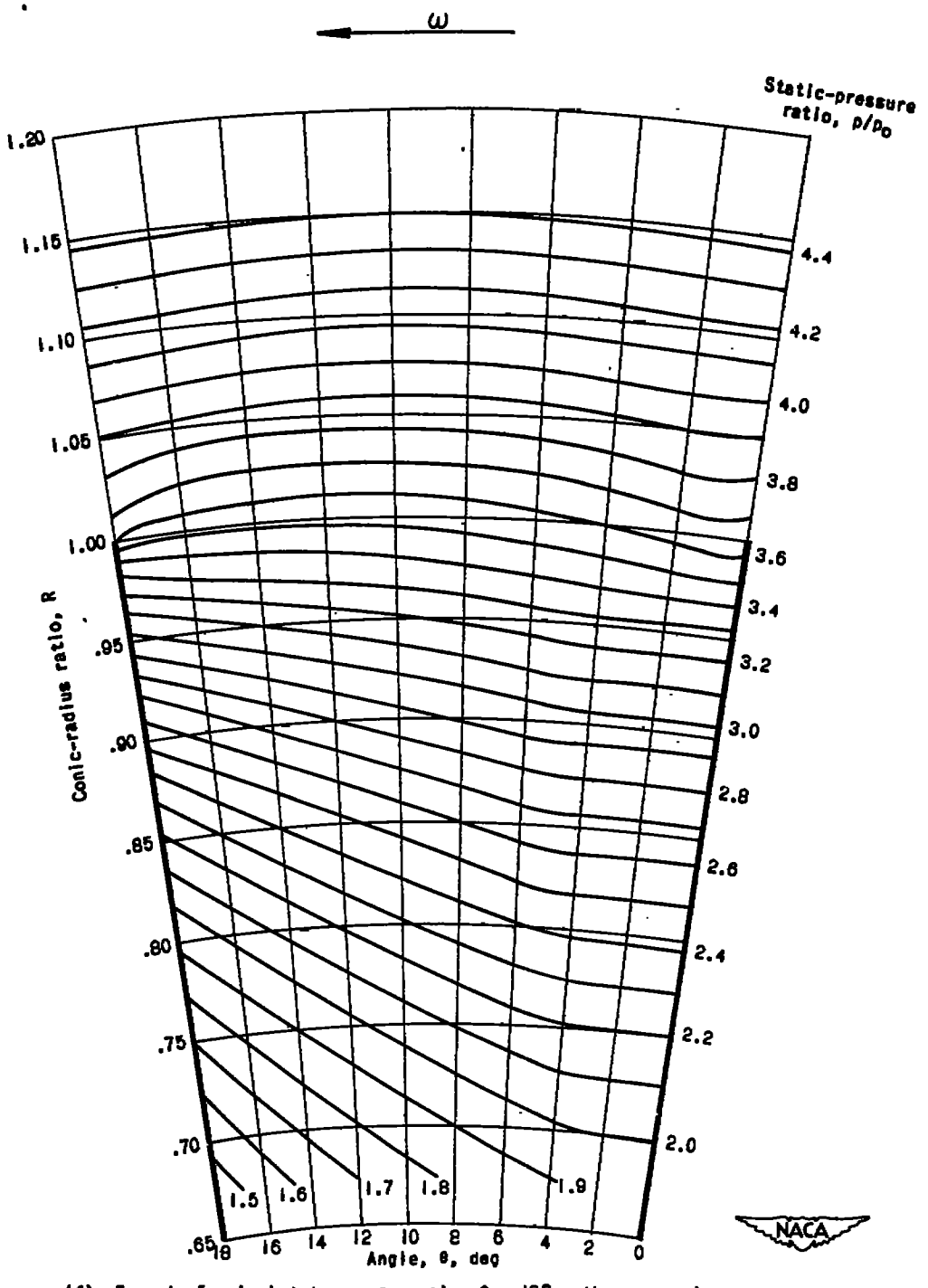

(f) Example 5: Included passage angle θ_t, 18°; other parameters same as standard example.

Figure 10. - Continued. Lines of constant static-pressure ratio.

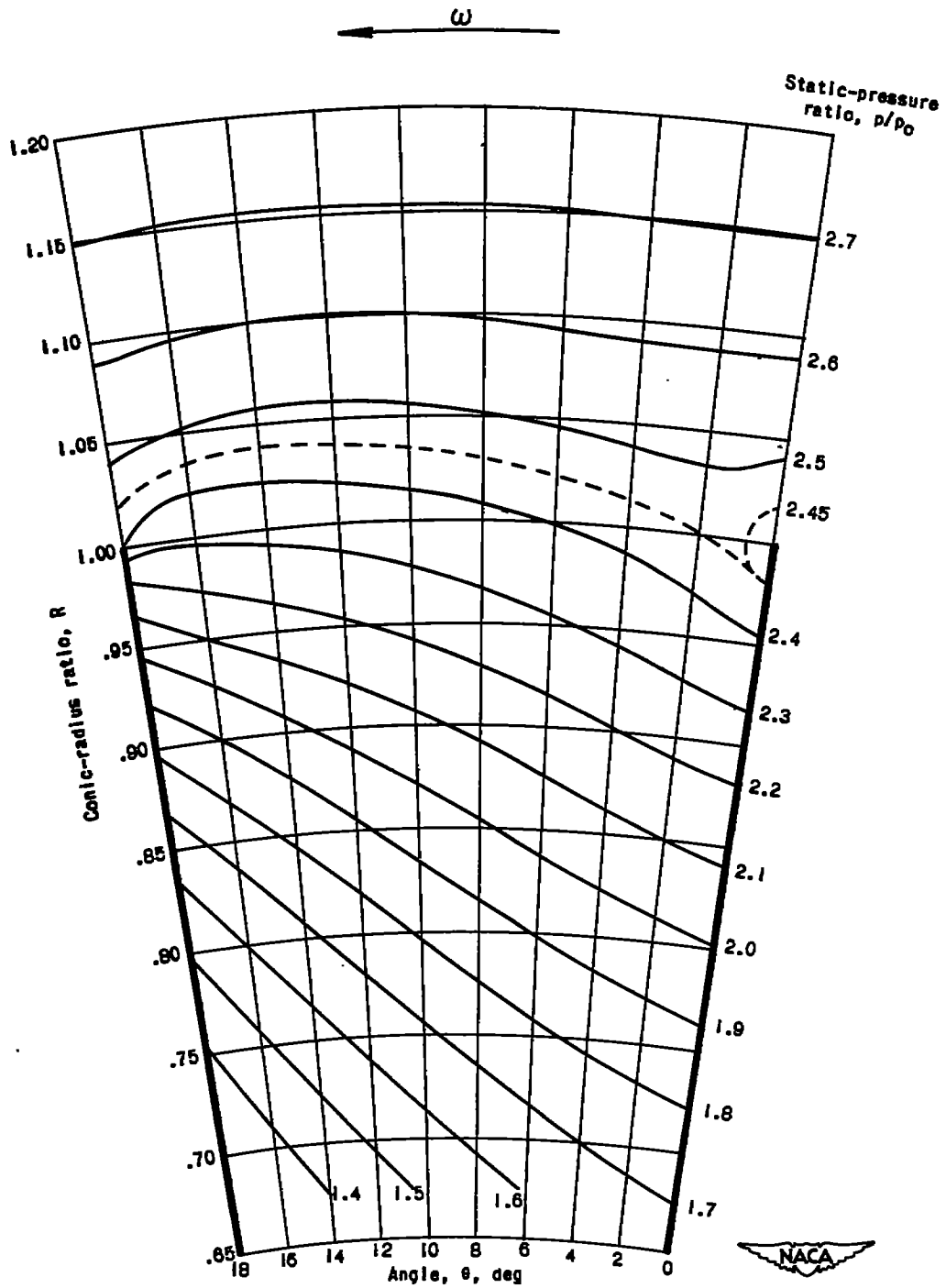

(g) Example 6: incompressible fluid; other parameters same as example 5 (fig. 10(f)). (Note that φ and M_T are based upon same constant c_0, the magnitude of which is equal to speed of sound at inlet conditions of example 5.)

Figure 10. - Concluded. Lines of constant static-pressure ratio.

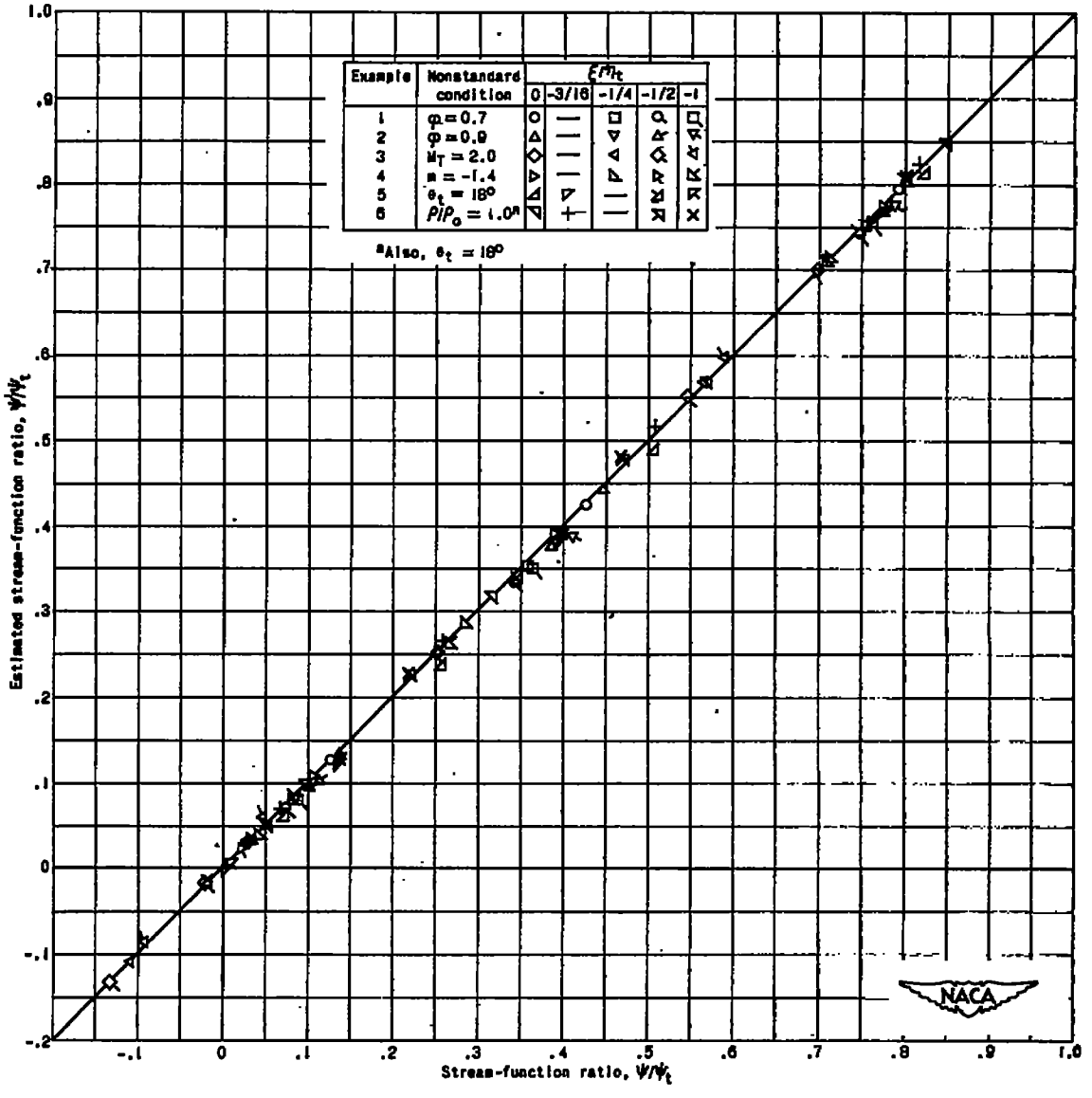

Figure 11. - Comparison between exact (relaxation solution) and estimated (correlation equation (B16)) values of stream-function ratio for various values of R (function of ξ/η_t and θ_t) and θ.

1147

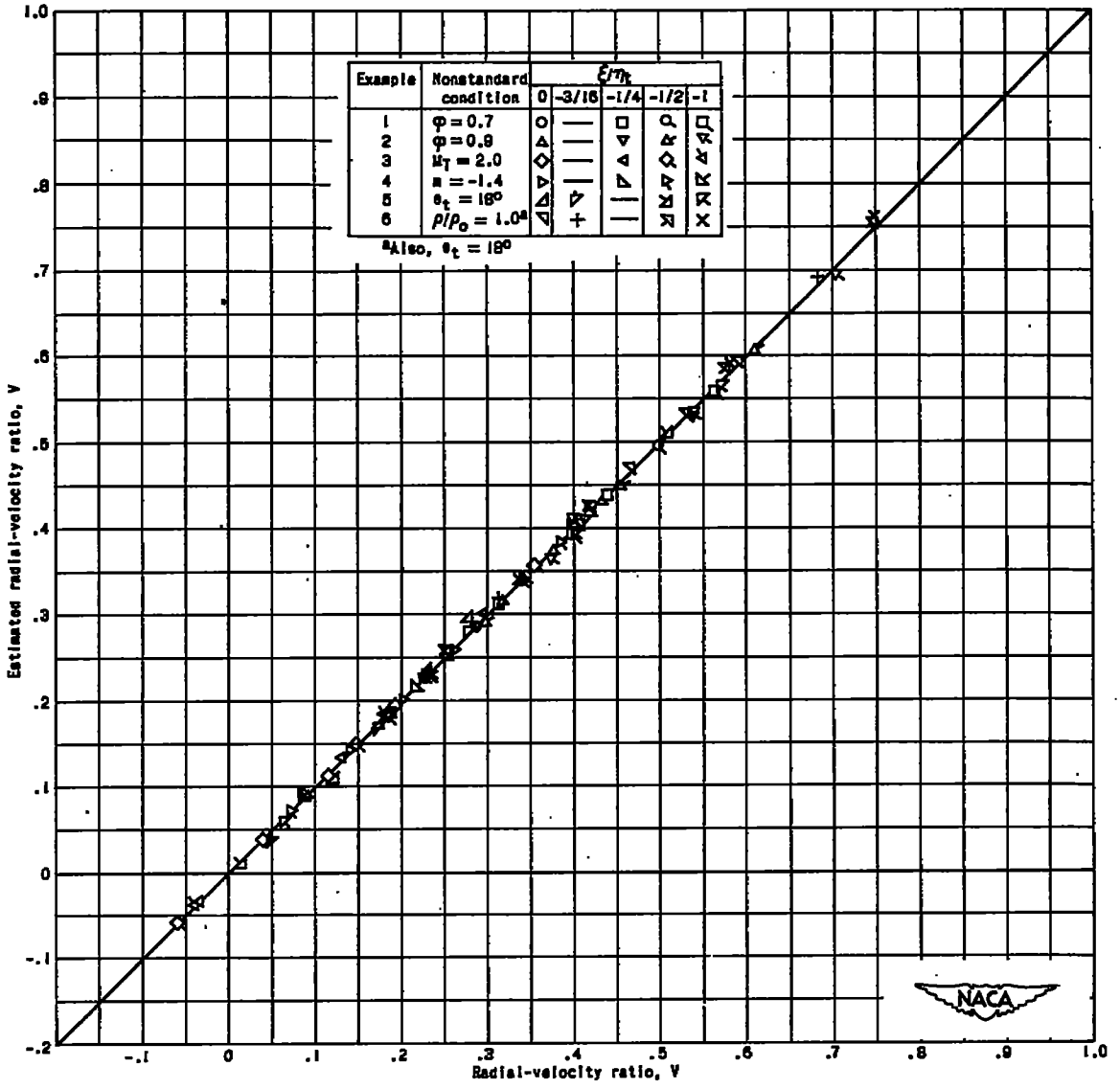

Figure 12. - Comparison between exact (relaxation solution) and estimated (correlation equation (B13)) values of radial-velocity ratio for various values of R (function of ξ/η_t and θ_t) and θ.

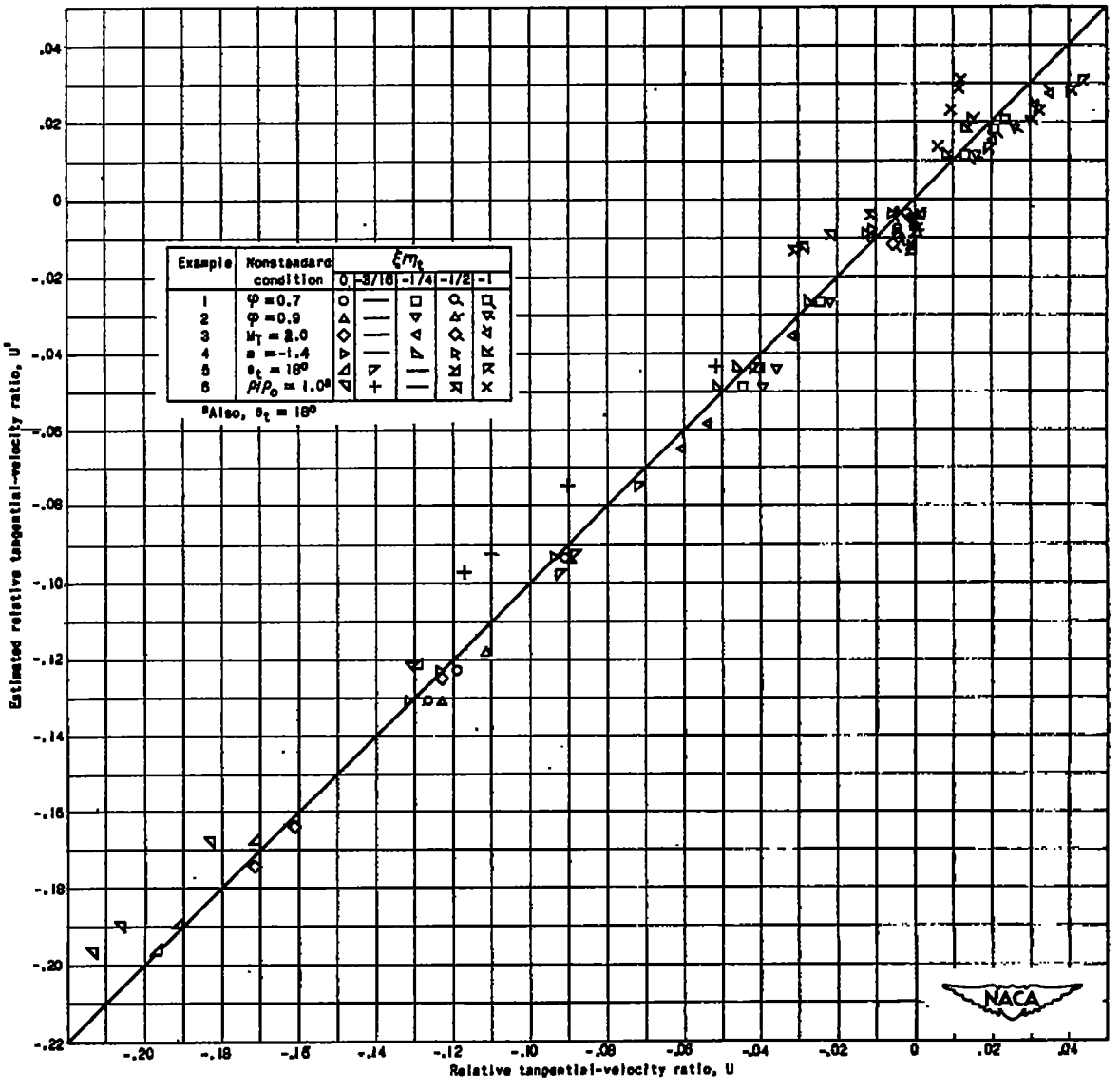

Figure 13. - Comparison between exact (relaxation solution) and estimated (correlation equation (B1)) values of relative tangential-velocity ratio for various values of R (function of ξ/η_t and θ_t) and s.

1147

1147

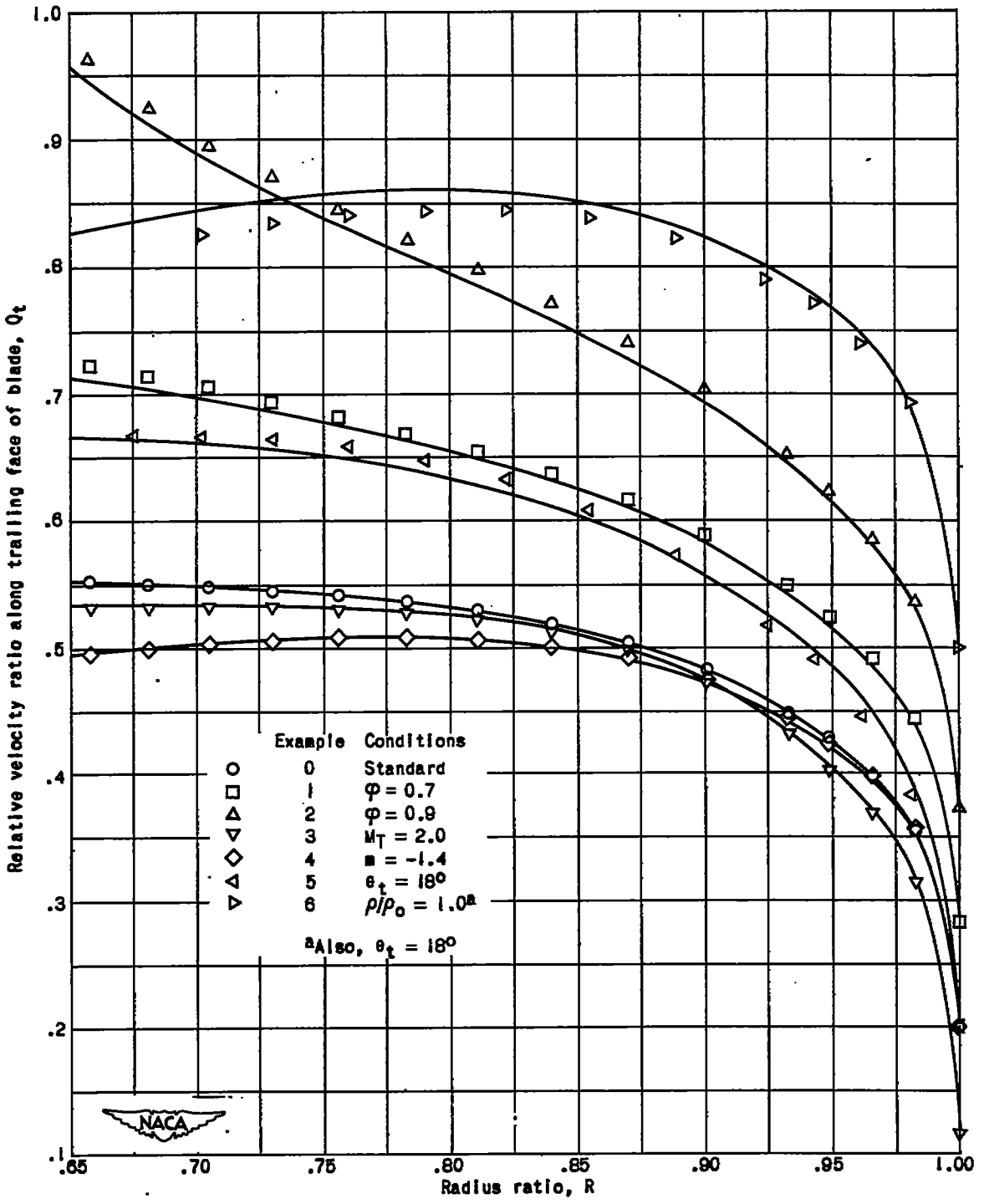

Figure 14. - Comparison between exact (relaxation solution) and estimated (correlation equation (B13)) values of relative velocity ratio along trailing face of blade. Solid lines obtained from correlation equation; plotted points obtained from relaxation solution.

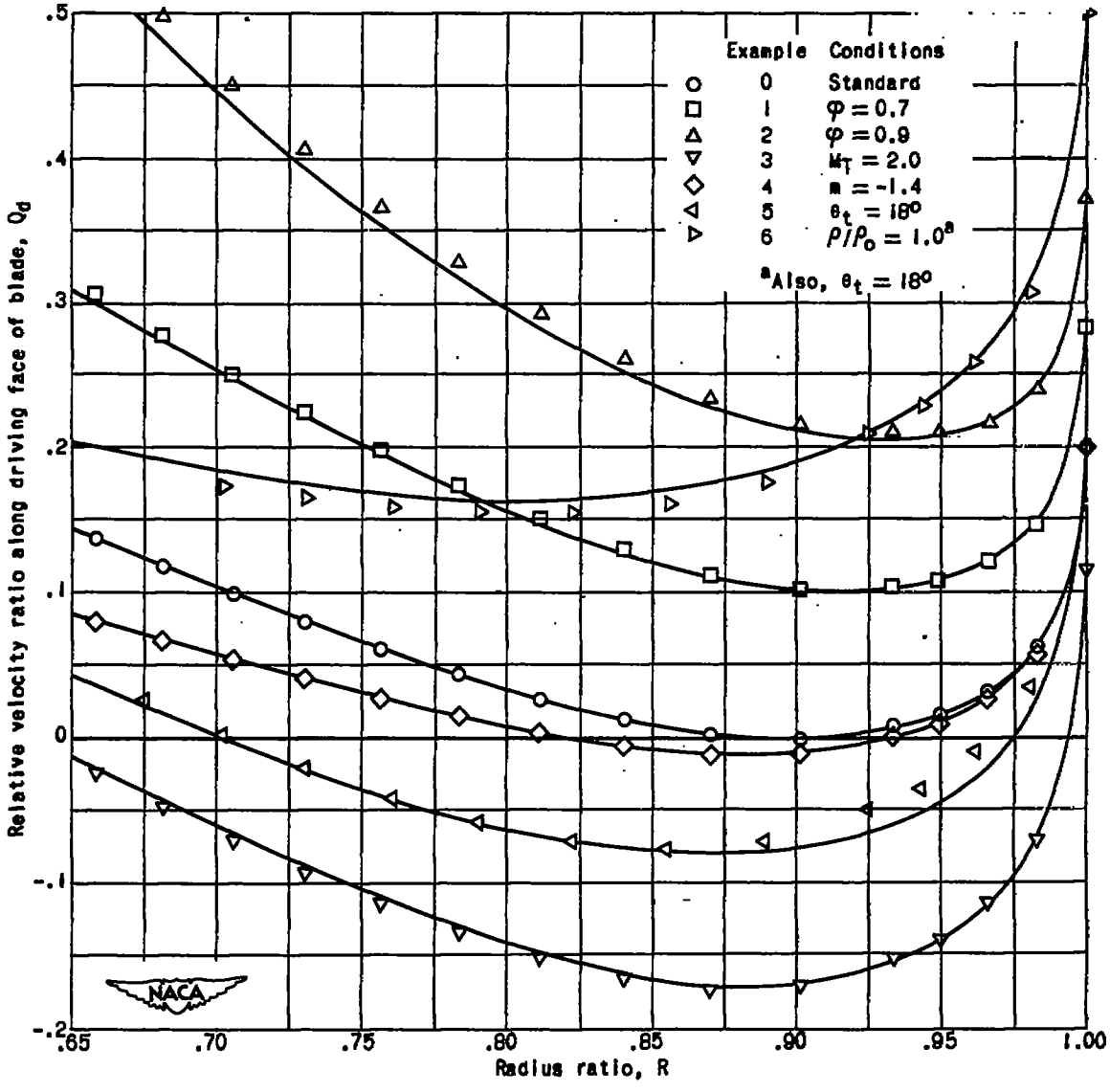

Figure 15. - Comparison between exact (relaxation solution) and estimated (correlation equation (B13)) values of relative velocity ratio along driving face of blade. Solid lines obtained from correlation equation; plotted points obtained from relaxation solution.

1147

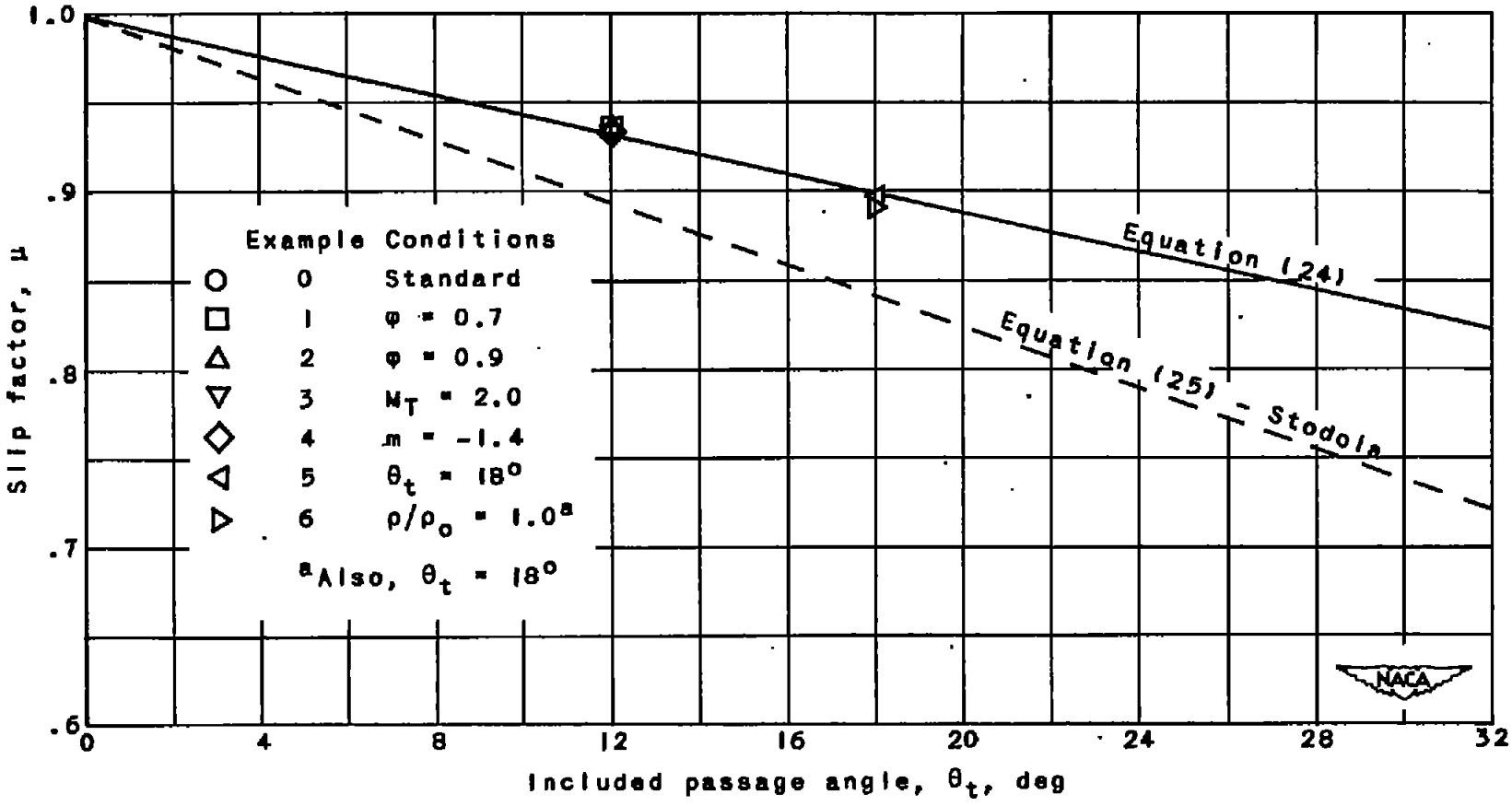

Figure 16. - Comparison among slip factors obtained from relaxation solutions, correlation equation (24), and Stodola's equation (25).

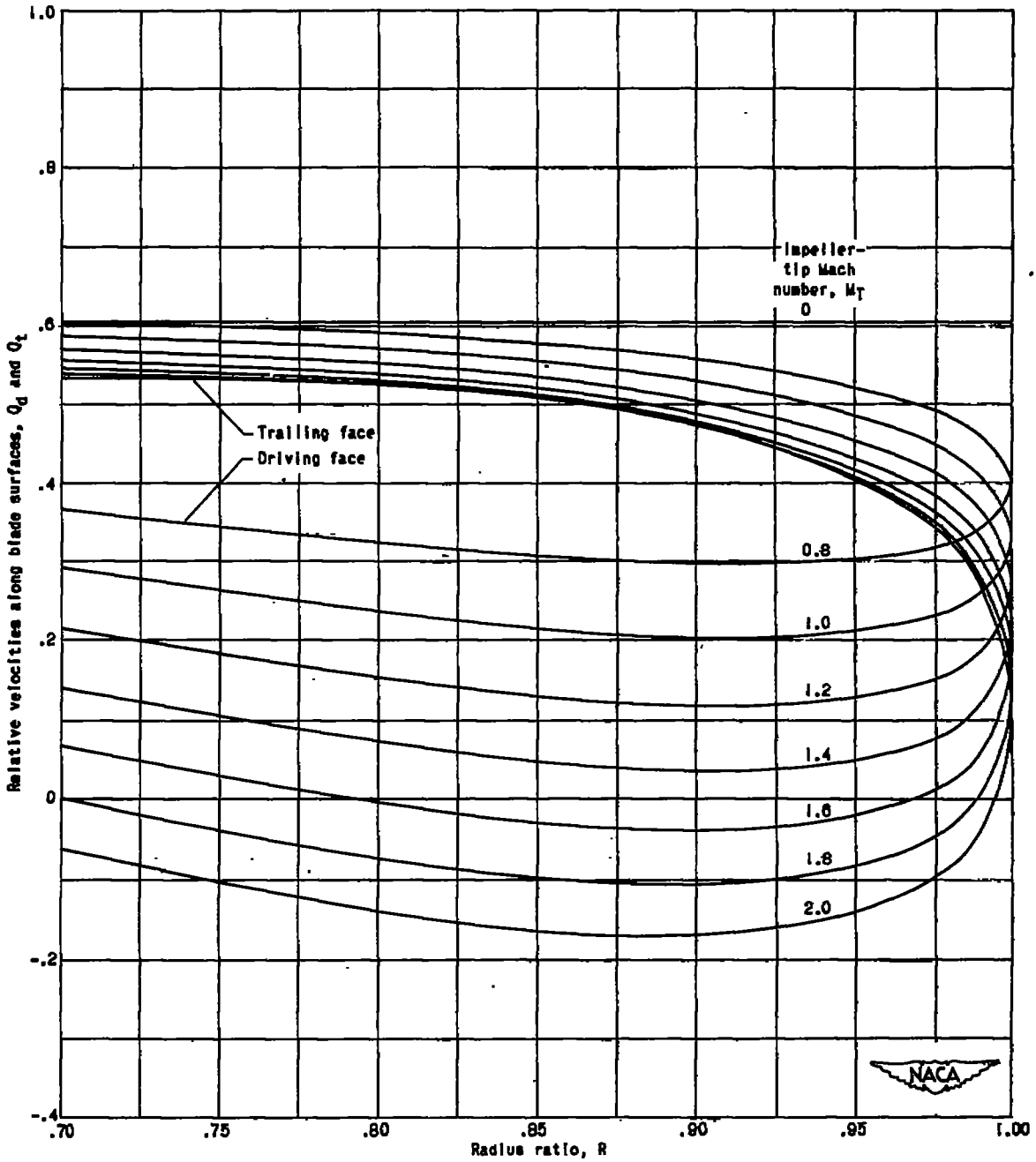

Figure 17. - Effect of impeller-tip Mach number upon relative velocity ratio along driving and trailing faces of blade. Correlation equation (B13); flow coefficient φ, 0.5; constant flow area (m, -1.0); included passage angle θ_t, 12°; compressible flow (γ, 1.4).

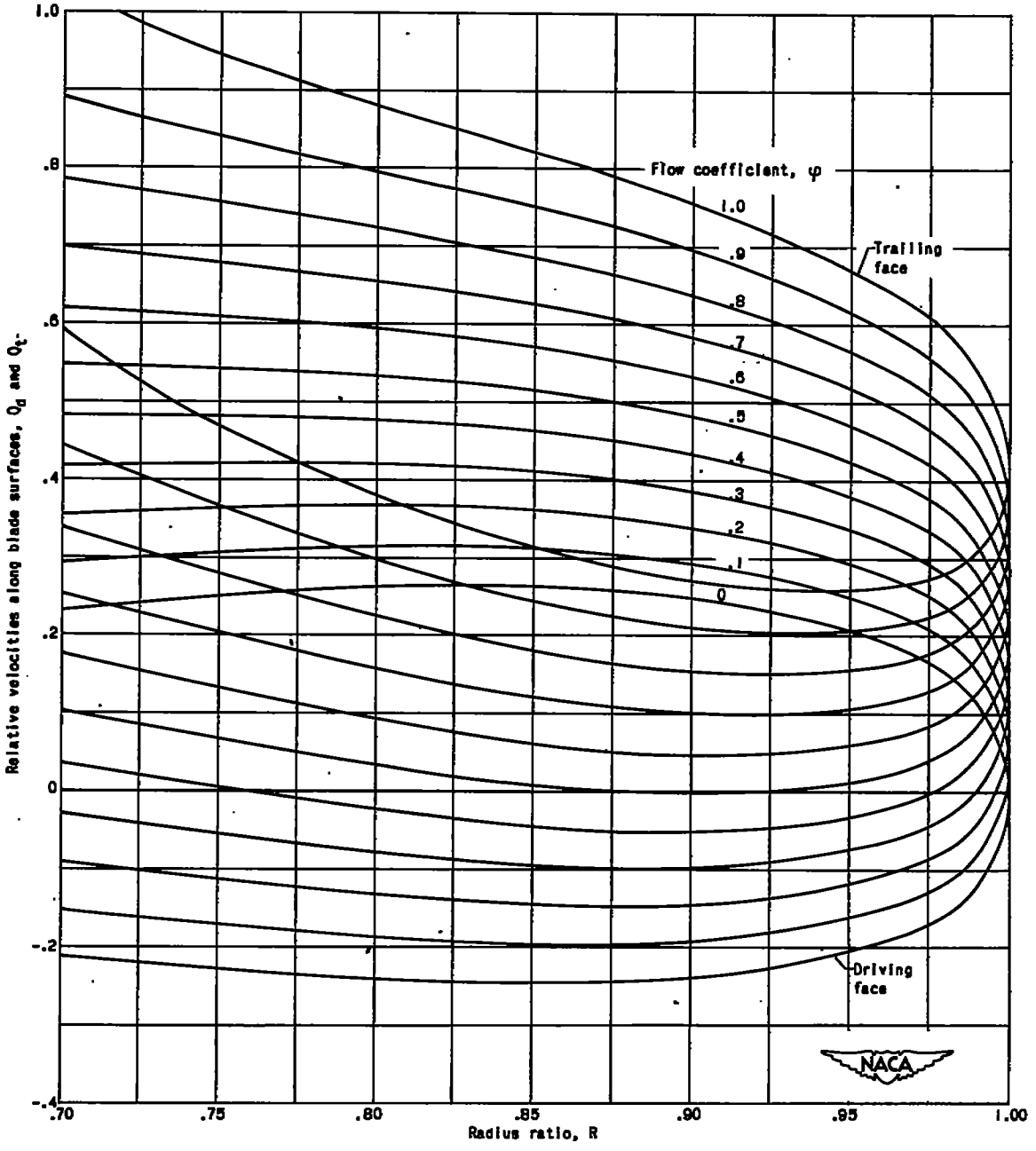

Figure 18. - Effect of flow coefficient upon relative velocity ratio along driving and trailing faces of blade. Correlation equation (B13); impeller-tip Mach number M_T, 1.5; constant flow area (m, -1.0); included passage angle θ_t, 12°; compressible flow (γ, 1.4).

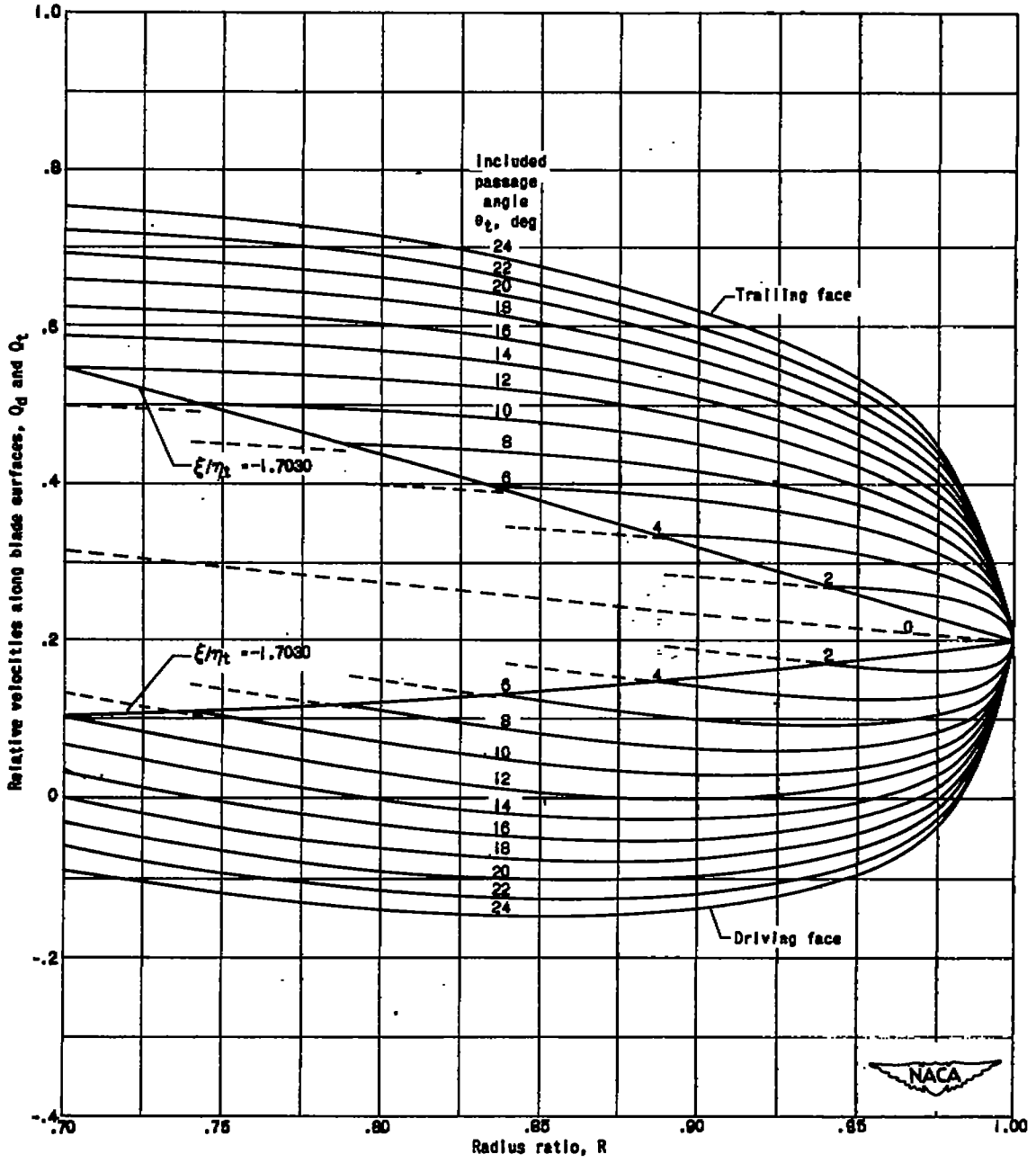

Figure 19. - Effect of included passage angle upon relative velocity ratio along driving and trailing faces of blade. Correlation equation (B13); dashed lines obtained from simplified analysis (equation (26)); flow coefficient φ, 0.5; impeller-tip Mach number M_T, 1.5; constant flow area (m, -1.0); compressible flow (γ, 1.4).

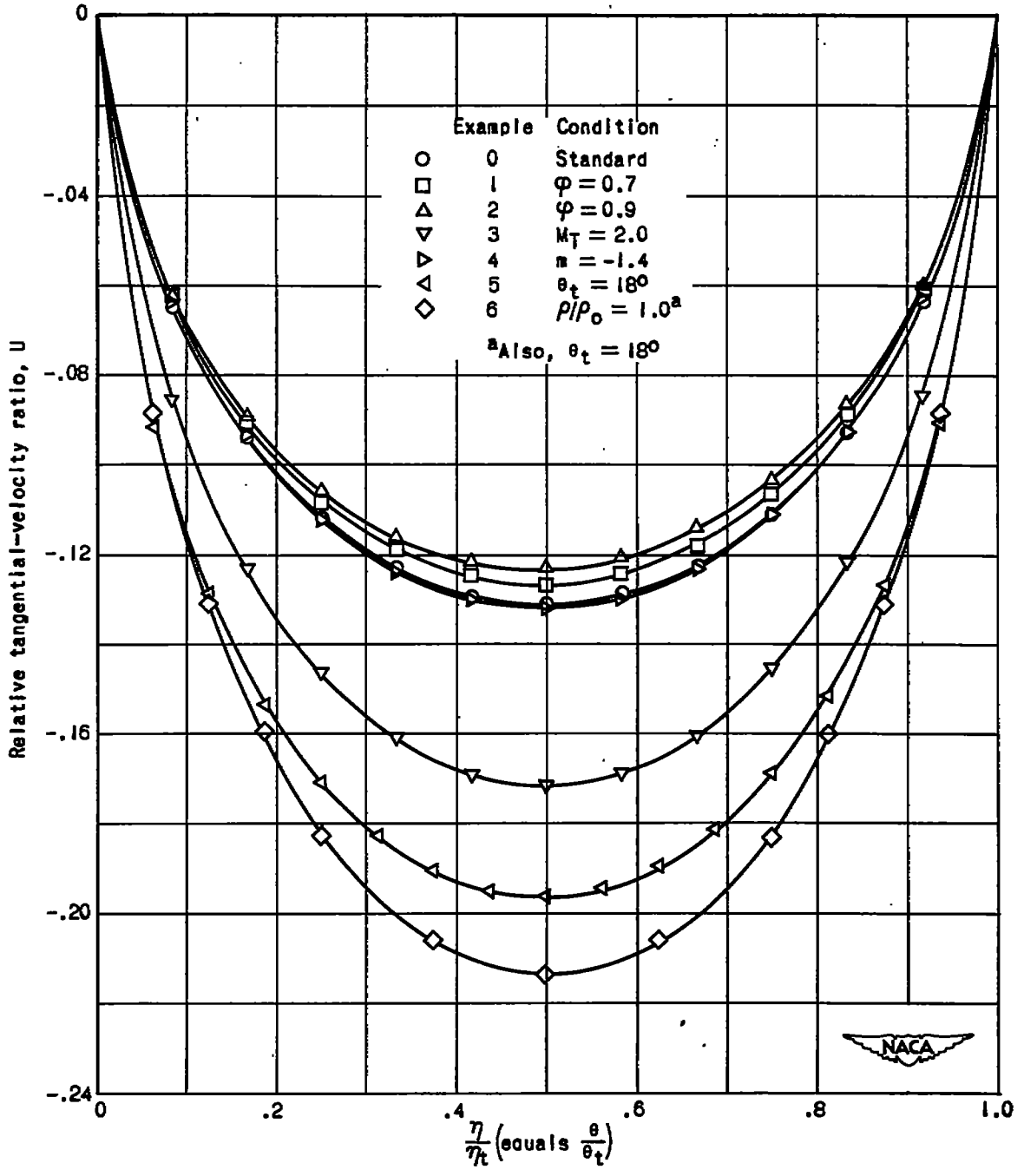

Figure 20. - Variation in relative tangential-velocity ratio across the impeller passage for $\xi/\eta_t = 0$. Plotted points obtained from relaxation solution.

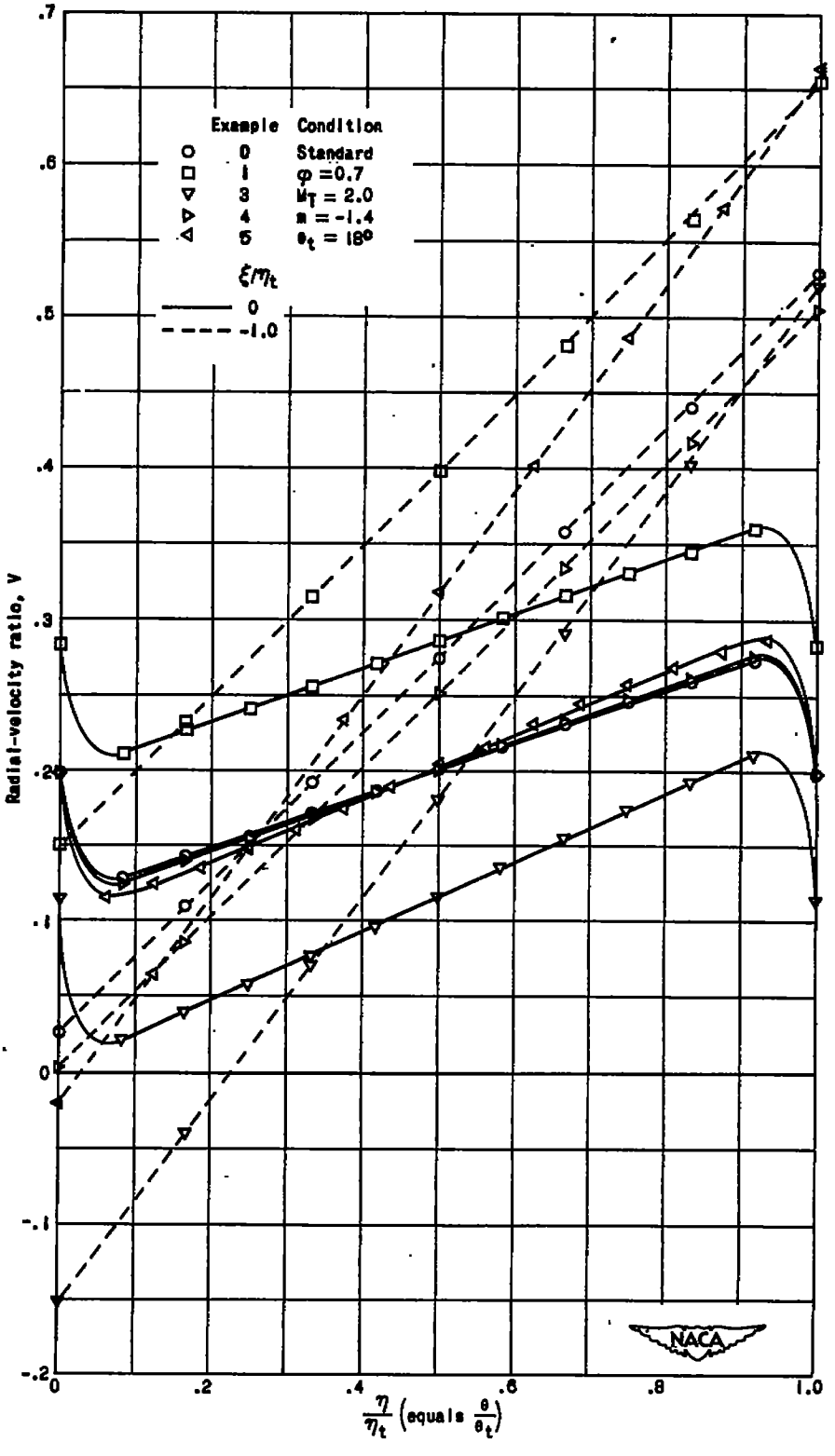

Figure 21. - Variation in radial-velocity ratio across the impeller passage for two values of ξ/η_t. Plotted points obtained from relaxation solution.